land

MDPI

Article

Capitalising on the Floristic Survey as a Non-Destructive Line of Evidence for Mineral Potential Modelling: A Case Study of Bauxite in South-Western Australia

Lewis Trotter [1,*], Grant Wardell-Johnson [2], Andrew Grigg [3], Sarah Luxton [4] and Todd P. Robinson [1]

[1] School of Earth and Planetary Sciences, Curtin University, Perth, WA 6845, Australia; t.robinson@curtin.edu.au
[2] School of Molecular and Life Sciences, Curtin University, Perth, WA 6845, Australia; g.wardell-johnson@curtin.edu.au
[3] Environment Department, Alcoa of Australia Ltd., Pinjarra, WA 6208, Australia
[4] Environment Division, Commonwealth Scientific and Research Organisation (CSIRO), Canberra, ACT 2601, Australia; sarah.luxton@csiro.au
* Correspondence: lewis.trotter@postgad.curtin.edu.au

Abstract: While geobotanists have long used plant occurrence to locate subsurface resources, none have utilised floristic surveys as evidence in models of mineral potential. Here, we combine plant species distributions with terrain metrics to produce predictive models showing the probability of bauxite presence. We identified nineteen taxa with statistically significant associations with known bauxite deposits and identified eleven terrain metrics from previous studies. We grouped variables into three variable sets (floristic, topographic, and topo-flora) and produced mineral potential models for each using four algorithms or approaches: (a) a generalised linear model (GLM); (b) random forest (RF); (c) maxent (ME); and (d) a heterogenous stacking ensemble (GLM-RF-ME). Overall, the random forest model outperformed all algorithms including the ensemble based on the area under the curve (AUC) metric. The floristic set of variables outperformed the topographic set (AUC: 0.86 v 0.82). However, together they had the greatest predictive capacity (AUC: 0.89). Six taxa, including *Banksia grandis*, *Leucopogon verticillatus*, and *Persoonia longifolia*, were indicators of bauxite presence, while five other taxa, including *Xanthorrhoea preissii* and *Hypocalymma angustifolium*, were associated with bauxite absence. Important topographic variables were topographic wetness, landscape position, and valley depth, which characterised bauxite locations as being well drained, in the upper slope positions of subdued hills, and at some distance from valleys. The addition of floristic surveys provides a new line of evidence about the overlying botanical life that tolerates, accumulates, or avoids bauxite or associated minerals. As opposed to drilling, both datasets can be collected and interrogated at low cost and without impact to the surrounding environment. These data are valuable additions to future applications of mineral potential modelling.

Keywords: bauxite; mineral potential modelling; geobotany; machine learning; topography; exploration; Jarrah Forest; kriging

Citation: Trotter, L.; Wardell-Johnson, G.; Grigg, A.; Luxton, S.; Robinson, T.P. Capitalising on the Floristic Survey as a Non-Destructive Line of Evidence for Mineral Potential Modelling: A Case Study of Bauxite in South-Western Australia. *Land* **2024**, *13*, 1995. https://doi.org/10.3390/land13121995

Academic Editor: Benjamin Burkhard

Received: 17 October 2024
Revised: 15 November 2024
Accepted: 21 November 2024
Published: 22 November 2024

1. Introduction

Geobotany is a form of mineral prospecting that utilises floristic surveys to assist in the identification of the location and extent of orebodies [1]. Geobotanists have long recognised the relationship between the distribution of vegetation and minerals in the substratum [2]. Plants that elucidate this relationship are broadly referred to as indicator plants [3], which either avoid, tolerate, or accumulate high concentrations of metals [4,5]. *Hydrangea macrophylla* is an example of a plant that tolerates aluminium, indicating aluminium availability by producing blue flowers if it is available and pink flowers if it is absent [6]. Many indicator species are well known, and a comprehensive list can be found

in Cannon [7] and Brooks [1]. Their identification is often achieved using geobotanical surveying and/or remote sensing techniques [8].

Modern exploration acknowledges that most exploitable deposits are becoming harder to identify with any one line of evidence [9]. Consequently, Geographic Information Systems (GISs) have been increasingly adopted to combine multiple lines of evidence into mineral potential models to enhance exploration [10]. Typically, the first step of this process involves sourcing multiple spatial layers (i.e., evidence) that conceptualise the mineralisation style and setting, such as faults and other lineaments, lithology, and geochemistry [11]. These layers are then associated and combined using a knowledge- or data-driven integration technique to create mineral potential maps. Knowledge-driven techniques rely entirely on expert opinion to select, weight, and integrate evidence layers. Prominent knowledge-driven techniques used in mineral prospecting include Boolean logic [12], fuzzy logic [13], and evidential belief [14]. Due to the subjective nature of knowledge-driven techniques, their application is typically reserved for when exploration data are scarce [15].

Data-driven techniques quantify spatial relationships between evidential features and known locations of mineral occurrence [15]. The resulting model is then used to infer mineral probability in unexplored areas. Historically, statistical methods such as Bayesian networks [16], logistic regression [17], and weight of evidence [18] were often used due to their ease of interpretation. In recent decades, machine learning algorithms have been increasingly used due to their ability to learn and model complex non-linear patterns from large datasets [19]. Algorithms such as artificial neural networks [20], maximum entropy [21], neural networks [22], random forest [23], and support vector machine [24] are amongst the most frequently utilised [25]. These techniques have been found to improve predictive performance over earlier statistical methods, which often struggle with non-linear correlations and large numbers of evidential inputs (e.g., [26,27]).

Mineral potential modelling generally combines geochemical, geological, geophysical, and remote sensing data as model evidence. These are selected to represent key geological and topographic factors that influence the formation of a mineral deposit type [10]. To the best of our knowledge, plot-based floristic data have never been included amongst this evidence. Instead, most GIS-based geobotanical prospecting focuses on remote sensing to map prospective areas. Most studies apply satellite imagery to map mineral-related spectral anomalies or patterns in broad vegetation canopies [28–30]. In some cases, multi-spectral vegetation indices are integrated with topographic and climatic maps to classify lithology [31,32].

Although also relatively uncommon in mineral potential modelling, topographic variables (e.g., slope, aspect, curvature) have been successfully used to assist in the identification of shallow mineral prospects. Ibanez et al. [33] used a public DEM to derive topographic position and wetness, terrain flatness and openness, and valley depth to map hydrocarbon prospects, and Carranza et al. [34] combined slope derivatives and geological evidence to model nickeliferous-laterite potential. Albrecht et al. [35] integrated many of these metrics with machine learning to target mineralised landscape units in Western Australia. Other studies have used topographic variables to derive ore-related structural lineaments [36,37] and stream sediments [38] for use in prospecting.

The ever-expanding selection of available data-driven machine learning techniques has led to new difficulties around model selection and optimisation [39]. This has led to proposals from both ecologists [40] and geologists [41] to consider a multi-model ensemble approach. Ensemble techniques integrate multiple independent models to reduce model overfitting, variance, and bias to improve overall prediction accuracy [42]. At present, ensemble methods include homogenous bagging and boosting frameworks that combine outputs from the same algorithm trained in different ways, and heterogenous stacking frameworks that combine different algorithm types [43]. In all frameworks, models make independent predictions, either in parallel or sequentially, and are then weighted by an evaluation metric and combined via averaging [44]. As such, ensemble methods can outperform single models [45] and are

receiving attention in ecology (e.g., [46]) and, more recently, in mineral potential modelling (e.g., [41,47,48]).

Nearly half of Australia's bauxitic alumina is mined in the Darling Range of south-western Australia [49]. However, the bauxite here is low-grade ore (c. 33% available alumina), typically obscured by under 1 m of overburden and well within the reach of most plants' root systems. As a prerequisite to mining, plot-based surveys to inventory all plant species in the area are a requirement [50]. We seek to harness the potential of these floristic data for geobotanical purposes and their combination with terrain metrics for retrospective prediction of bauxite occurrence in this area. We have two aims: (a) statistically identify variables for the prediction of bauxite based on floristic surveys and topography; and (b) combine variables using mineral potential modelling to predict the likelihood of bauxite presence. We explore the potential of floristic surveys and topographic variables individually and in combination using three alternative modelling techniques and an ensemble approach. The contribution of each variable in the final model is discussed.

2. Materials and Methods

2.1. Study Area

This study was conducted within a subset (c. 89,000 ha) of Alcoa's Huntly bauxite mine, located in the Northern Jarrah Forest subregion of the Darling Range, Western Australia (Figure 1). Mining commenced here in early 2000 and is ongoing. The topography of the region is an undulating plateau averaging 300 m above sea level, with frequent and widespread upland hills and deeply incised valleys [51]. The study area experiences a Mediterranean climate with cool winters and warm summers and is situated in the western parts of the Darling Range where annual rainfall exceeds 1000 mm [52]. Vegetation predominantly consists of dry sclerophyll forest with an overstorey dominated by *Eucalyptus marginata* (jarrah) and *Corymbia calophylla* (marri), and a midstorey of *Banksia grandis* (bull banksia) and *Allocasuarina fraseriana* (sheoak). Species diversity is exceptionally high, comprising c. 800 species and 21 broad vegetation types [53,54].

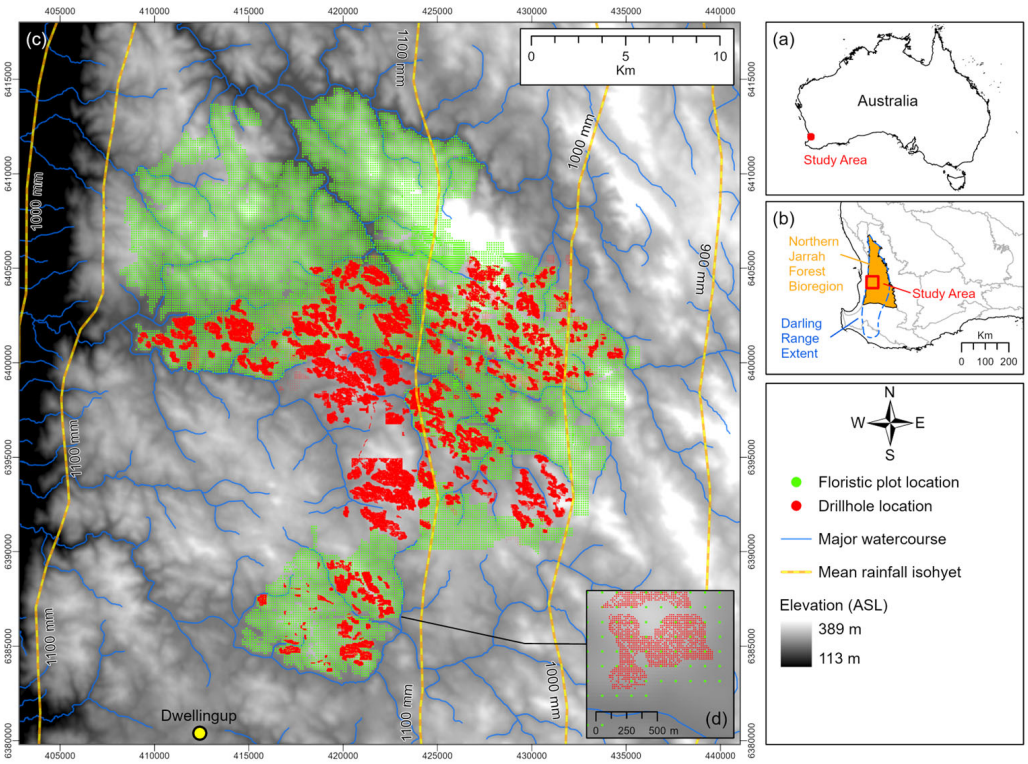

Figure 1. Location of (**a**) the study area situated within a subsection of Alcoa's Huntly bauxite mine occurring within (**b**) the Northern Jarrah Forest subregion of the Darling Range, Western Australia.

The study area falls predominantly within a high rainfall zone exceeding 1000 mm per annum. The extent of (**c**) all floristic plots and bauxite exploration drillholes used in analysis, as well as (**d**) a closer view showing a smaller subset, are provided. Background shows a digital elevation model at 30 m resolution acquired from the Shuttle Radar Topography Mission (SRTM).

2.2. Conceptual Model

A conceptual model of Darling Range lateritic bauxite is shown in Figure 2 (after [55]). The key characteristics are summarised as follows:

- Orebodies are restricted to the upland geomorphology of the region between 250 and 350 m above sea level [56].
- Individual orebodies are discontinuous, generally lenticular in shape and elongate northwest, vary up to 80 ha in areal extent, and can attain a thickness of 13 m at Huntly [55].
- High rainfall promotes bauxitisation by enabling desilication and the alteration of clay minerals to bauxite minerals, and stabilises soil acidity [57,58]. As such, higher-grade ore occurs in the west of the Darling Range where rainfall is high (c. 1100 mm annually) and declines as rainfall reduces inland [59].
- Granite and dolerite parent rocks have physically produced the subdued topography (i.e., low hills) and upland geomorphology ideal for lateritic weathering [55,60].
- Thicker, better-quality orebodies tend to occur on mid- to upper-hill slope gradients where the movement of water is optimal for draining byproducts from weathered areas, for lower groundwater levels that inhibit formation, and for preventing stagnant soil conditions and waterlogging [61,62].
- Bauxite is thin or absent on hill crests and lower valley slopes due to low slope gradients and sluggish drainage [55].

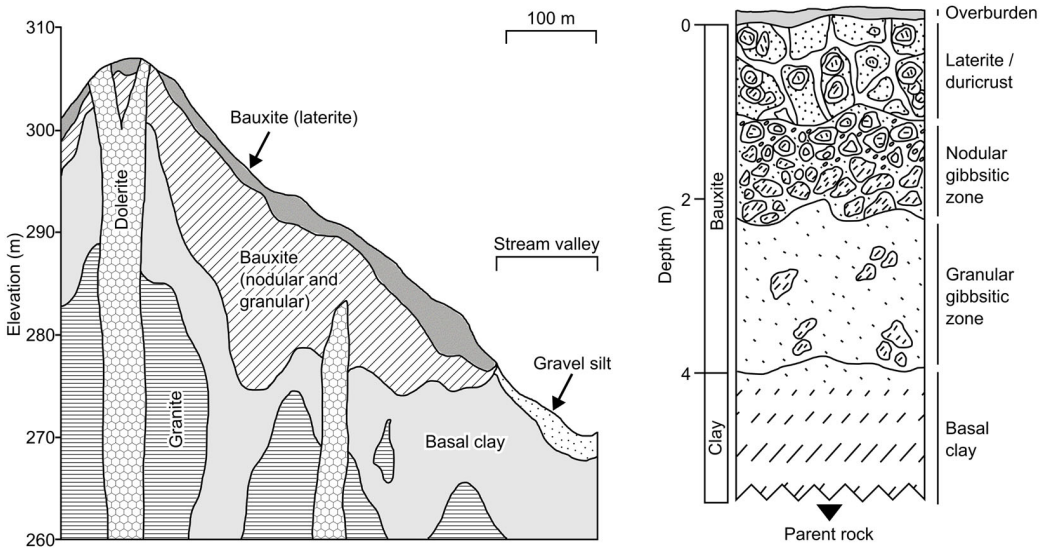

(**a**) (**b**)

Figure 2. Conceptual model of Darling Range lateritic bauxite geomorphology (**a**) and mineralogical profile of a typical high-grade deposit (**b**) (reinterpreted from the work of [55]).

2.3. Data Preparation

2.3.1. Bauxite Deposit Drillhole Data

Orebody exploration drilling is first undertaken on a uniformly spaced 120 × 120 m exploration grid, where vertical geochemistry samples (c. 6 m depth) are collected and analysed for available alumina, ferric oxide, reactive silica, and organic carbon quantities. Further drilling is undertaken on a 60 × 60 m grid to demarcate orebodies, followed by on

a 15 × 15 m grid for precision modelling where deposits are economically significant [55]. This information has been actively stored and managed in a spatial database by Alcoa since the 1970s. A subset of c. 170,000 drillholes captured between 2000 and 2015 from the Huntley mining region was used for this study (Figure 1c). Each record contains a coordinate, sampling date, and a categorical value representing generalised bauxite grade and extraction acceptability based on internal Alcoa algorithms (Table 1). We reclassified categories 1 and 2 to represent economic bauxite presence (1) and category F to represent bauxite absence (0) using ArcGIS Pro (v3.0.0; [63]). Categories M and U were excluded. Finally, bauxite locations were spatially thinned to 120 m to match the floristic plot exploration grid and reduce sampling bias [64].

Table 1. Drillhole-derived bauxite grade and extraction suitability categories.

Suitability Category	Description	Count
1	Accepted drillhole based on bauxite grade and deposit depth.	81,407
2	Accepted drillhole based on deposit depth.	16,280
M	Unaccepted drillhole based on insignificant ore.	5373
U	Unaccepted drillhole based on user reassessment.	104
F	Unaccepted drillhole based on bauxite grade and deposit depth.	66,818

2.3.2. Floristic Plot Data

To meet statutory requirements, Alcoa has actively undertaken plot-based floristic surveys in pre-exploration forest areas since 1991. Plots are based on the same 120 × 120 m exploration grid used during exploration drilling. At each plot, a coordinate and a sampling date are recorded, along with an inventory of all understorey and overstorey species within a 5 m and 20 m radius, respectively. These data were provided by Alcoa in various spreadsheet files that were cleaned and standardised using the Floristic Information Management System [65], resulting in c. 31,000 forest plots over an area of 43,200 ha, comprising 469 taxa from 260 genera. Further filtering was conducted to remove unverified and non-perennial species, and species with less than 100 observations. Finally, plots were spatially clipped to the drillhole dataset extent, leaving c. 25,000 plot records comprising 105 taxa for use in analysis (Figure 1c).

2.4. Model Variables

2.4.1. Indicator Plant Species

Each plot location was spatially joined to the nearest neighbouring bauxite drillhole location within a 120 m search radius, thereby attributing plant species with bauxite presence/absence information. A Chi-squared statistic was used on each species to test for a significant association ($\alpha = 0.05$) with bauxite presence and absence locations [66]. Plant species that were significantly associated with presence or absence were interpolated into continuous raster surfaces representing a probability of occurring within each cell [0, 1] using kriging. We chose disjunctive kriging over other linear interpolators such as ordinary kriging due to its ability to handle non-parametrically distributed, binary (i.e., presence/absence) data [67]. Additionally, disjunctive kriging was chosen over the comparable indicator kriging technique, as indicator kriging is ultimately a nested disjunctive kriging interpolator [67]. We used the Geostatistical Analyst extension in ArcGIS Pro (v3.0.0; [63]) to perform exploratory analysis and disjunctive kriging on each species following an approach outlined in [68]. We used an omni-directional semi-variogram fitted with a stable model, with all other parameters optimised by the Geostatistical Analyst extension, to perform disjunctive kriging. Prediction performance was assessed using leave-one-out cross-validation based on root-mean-square error measures [69] (see Table A2).

2.4.2. Topographic Variables

We used the 1 s (c. 30 m) hydrologically enforced digital elevation model (DEM) obtained from the Shuttle Radar Topographic Mission (SRTM; [70]) shown in Figure 1c, along with SAGA software (v8.0.0; [71]), to derive topographic variables representing bauxite formation and distribution controls identified by Hickman et al. [55]. The SRTM DEM was captured in February 2000, which predates mining that commenced in mid-2000.

A range of topographic variables were included to explore deposit shape, orientation, and position (Table 2). Aspect was used to consider the northwest orientation of deposits, which we calculated in degrees and converted to continuous "eastness" (ASE) and "northness" (ASN) variables as per Amatulli et al. [72]. Mean curvature (MCV), which combines convexity and concavity to summarise overall surface curvature [73], was included to provide evidence for lenticular-shaped deposits. We also derived the relative landscape positions of deposits from their immediate surroundings using the multiscale topographic position index (mTPI). The mTPI combines the topographic position index [74] at multiple scales to better represent local and global topography [75]. Similarly, we used valley depth (VD), which is calculated as the difference between the elevation and an interpolated global ridge level [71], to measure the negative association between bauxite grade (and occurrence) and proximity to lower hills and valley areas.

Table 2. Topographic variables used to represent bauxite formation and distribution controls.

Variable Name	Abbreviation	Description	Citation
Aspect Eastness	ASE	Aspect as ranging from −1 to 1 representing west and east slopes, respectively.	[76]
Aspect Northness	ASN	Aspect as ranging from −1 to 1 representing south and north slopes, respectively.	[76]
Downslope Distance Gradient	DDG	Measure of hydraulic gradient. Lower gradient on concave slopes, higher when convex.	[77]
Mean Curvature	MCV	Overall surface curvature. Low values are accumulation areas, high values are denudation.	[73]
Mid-Slope Position	MSP	Isolates mid-slope position of hills. Mid-slope is 0 and value increases further away from mid-slope.	[78]
Multi-Resolution Ridge Top Flatness	mRTF	Identifies flat ridge areas. Values closer to 1 are perfectly flat hill tops.	[79]
Multi-Resolution Valley Bottom Flatness	mVBF	Identifies flat valley areas. Values closer to 1 are perfectly flat valley bottoms.	[79]
Multiscale Topographic Position Index	mTPI	Terrain position at multiple scales. Hills are positive values, valleys are negative. Plains are 0.	[74]
SAGA Wetness Index	SWI	Topographic controls on hydrology. Higher values are high wetness and accumulation.	[80]
Valley Depth	VD	Distance from interpolated ridge line to valleys. Higher values are deeper valleys.	[81]
Wind Exposition	WE	Terrain exposure to wind. Lower values are sheltered terrain, higher values are more exposed.	[82]

Associations between bauxite and hill slopes were also examined. The mid-slope position (MSP) index was used to isolate mid-slope gradients along hills [83], where bauxitic weathering is most efficient, and multi-resolution ridge top flatness (mRTF) and

valley bottom flatness (mVBF) indices [79] were used as evidence for bauxite-inhibiting flat hill crests and valleys. To quantify drainage intensity and water accumulation, we used the SAGA wetness index (SWI). The SWI represents soil wetness and is calculated using the topographic wetness index [84] with improved catchment calculation [71]. The hydrological downslope distance gradient (DDG) metric was also included to further investigate the impact of local slope characteristics on runoff [77]. Finally, we used the wind exposition (WE; [82]) index to determine if climate-exposed parts of the landscape promote bauxite due to increased access to meteoric water from rainfall and therefore drainage.

2.4.3. Multicollinearity Analysis

The usdm package (v2.1.7; [85]) in R (v4.3.0; [86]) was used to calculate the Pearson correlation coefficients and variance inflation factor (VIF) for each variable against all others, as recommended by Cobos et al. [87]. To assess the multicollinearity of flora and topography separately, we calculated the VIF for three sets: all topographic variables only (Set 1), all flora variables only (Set 2), and all variables combined (Set 3). As highly correlated variables can cause unstable model estimates, we removed significant correlates from each group using backward stepwise elimination based on the variable with the highest VIF [85]. We applied this technique to each set and only retained variables for which the VIF ≤ 3 based on Schwager and Berg [76].

2.5. Mineral Potential Modelling

Mineral potential modelling was performed in R using the biomod2 package (v4.2.0; [88]). Modelling was undertaken via a multi-step procedure based on Schwager and Berg [76,89] that was applied to each of the three sets of variables independently. First, five sets of 10,000 pseudo-absence locations were randomly generated. Then, modelling was performed using generalised linear models (GLMs), random forest (RF), and maximum entropy (ME) algorithms. The GLMs were calibrated using logistic regressions with quadratic terms and one-way interactions due to the binomial distribution of the response variable. The RF and ME models used the biomod2 'untuned' setting, which implements the default options of the original algorithms [88]. Model training and validation were conducted via five internal cross-validations, where 80% of the data were randomly assigned for training and 20% for validation per iteration. Five permutations were used to measure variable importance per model, and validation was assessed via the area under the curve (AUC) metric obtained from the Receiver Operating Characteristic (ROC) curve. A ROC curve is a graph that represents how well a machine learning model performs by plotting the True Positive Rate (TPR) and False Positive Rate (FPR) at different classification thresholds; the TPR represents the proportion of actual positives correctly identified by the model, while FPR is the proportion of actual negatives incorrectly identified as positives by the model [90]. Additionally, the ROC curve can be used to generate the AUC statistic, which provides a summary measure of overall model performance, where an AUC of 0.5 is random, 1 indicates perfect model fit, and values between 0.7 and 0.9 are generally considered moderate to good [91,92]. An ensemble model integrated all three algorithms by combining the mean of probabilities of all model outputs with an AUC > 0.8. Bauxite potential maps were generated from the predictions of each model.

2.5.1. Variable Reduction and Model Optimisation

We reduced potential model overfitting and optimised model complexity by removing the maximum number of redundant predictor variables without a significant reduction in model AUC [93]. Redundant variables were eliminated through a stepwise process in which the least important variable was removed, the model was re-run, and the resulting AUC was statistically compared to the initial model using a DeLong test [94] using the pROC package (v1.18.1; [95]) in R. Variables were removed until the DeLong test determined a statistically significant ($p < 0.05$) difference in AUC. To ensure that model AUCs were consistent across iterations, we set aside 1000 randomly selected bauxite drillhole and pseudo-absence locations for evaluation purposes and used these to validate models during

the stepwise process. We applied this method to the three sets of variables. Finally, we used a Wilcoxon–Mann–Whitney test to determine if the model AUC values were statistically different ($p < 0.01$) between variable sets. We chose the Wilcoxon–Mann–Whitney test due to its use in comparing mean AUCs between several ensemble models in comparable studies [76,89].

2.5.2. Variable Response Curves

We generated response curves to evaluate model plausibility and to determine how variables interacted with bauxite potential [96]. Response curves plot the relationship between the probability of occurrence of a dependent variable (i.e., bauxite potential) and each of the predictor variables. For each plot, the response (y-axis) is modelled using one predictor (x-axis) while all others are held constant at their mean [96]. We used biomod2 [88], which implements the Evaluation Strip method [97] with the mean statistic for setting variables to a fixed constant. Response curves were created for each topo-flora variable that was retained after the model optimisation procedure per algorithm (GLM, RF, ME) within the final heterogenous ensemble.

3. Results

3.1. Model Variables

3.1.1. Indicator Plant Species

Nineteen species were found to be statistically associated with bauxite presence or absence based on Chi-squared tests (Figure 3). *Allocasuarina fraseriana* (sheoak) favoured bauxite presence more than all other species, with 62% of its 1555 occurrence records situated on bauxite orebodies. In contrast, five species had obvious statistically significant associations with bauxite absence. *Taxandria linearfolia* (swamp peppermint), *Eucalyptus patens* (yarri), *Hypocalymma angustifolium* (white myrtle), and *Hakea lissocarpha* (honey bush) occurrences (totalling 226, 405, and 490, respectively) were each situated off bauxite deposits over 70% of the time. *Xanthorrhoea preissii* (grass tree), an abundant and widespread species, also strongly favoured bauxite absence, with 65% of its 1157 records occurring off-deposit.

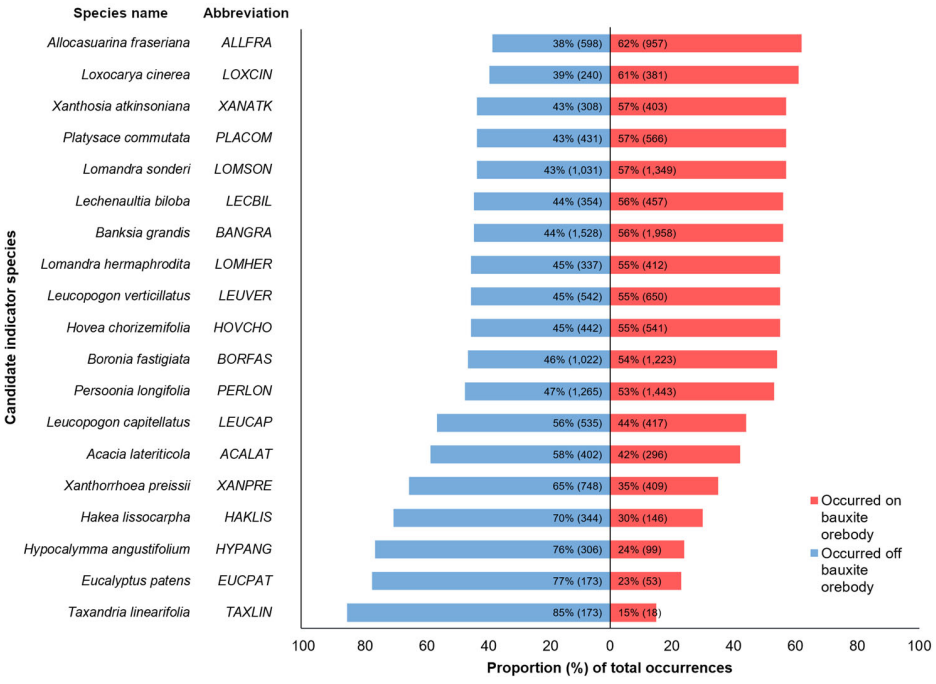

Figure 3. Nineteen plant species selected as candidates for bauxite prospectivity modelling. Species with significant associations with known bauxite deposits were identified using the Chi-squared statistic ($\alpha = 0.05$). The numbers in brackets represent the total number of plants occurring on and off bauxite that were considered in the Chi-squared analysis.

Plant species with prominent inclinations towards bauxite deposit presence (*Banksia grandis*) and absence (*Taxandria linearfolia*), represented in occurrence probability maps that were produced from disjunctive kriging, are presented in Figure 4.

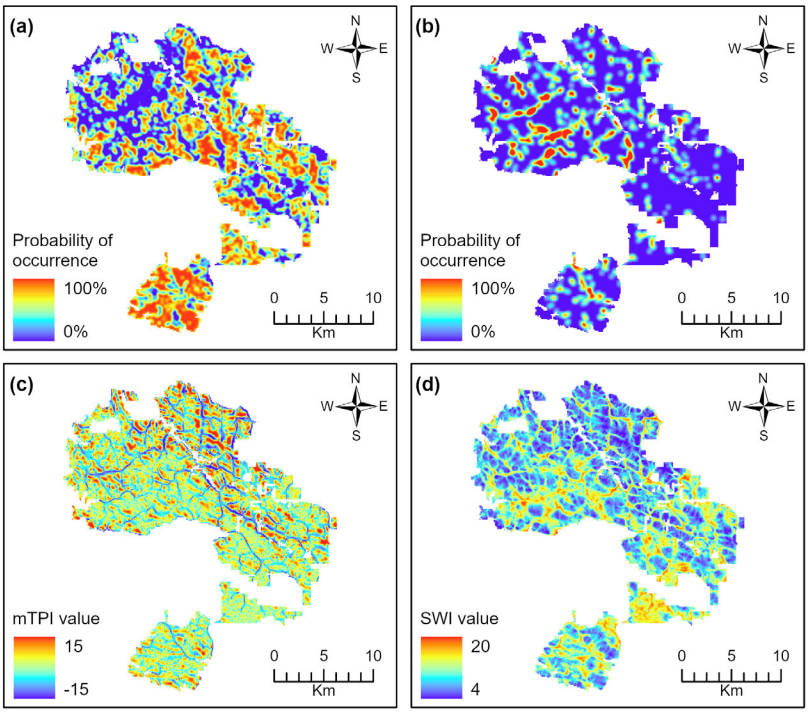

Figure 4. Exemplar plant species (**a**) *Banksia grandis* and (**b**) *Taxandria linearfolia* represented in occurrence probability maps resulting from disjunctive kriging. *Banksia grandis* is strongly positively associated with bauxitic presence, while *Taxandria linearfolia* is strongly negatively associated. Higher values of the topographic variables (**c**) multiscale topographic position index (mTPI) and (**d**) SAGA wetness index (SWI) were also found to strongly highlight bauxite-present and -absent areas, respectively.

3.1.2. Topographic Variables

Eleven topographic variables representing deposit shape, orientation, position, and topo-drainage processes were successfully derived from the SRTM DEM (shown in Figure 1c). The multiscale topographic position index (mTPI) was particularly notable for capturing the gentle undulating hills where bauxite frequently occurs (Figure 4c), while the SAGA wetness index (SWI; Figure 4d) was vital for highlighting the more mesic locations in the landscape, such as lower hill slopes and valley floors, where bauxite formation is generally inhibited.

3.1.3. Multicollinearity Analysis

The topographic derivatives (Set 1) mean curvature (MCV), multiscale topographic position index (mTPI), SAGA wetness index (SWI), and wind exposition (WE) exhibited high pairwise correlations (i.e., VIF > 3; Figure A1). Based on the backward stepwise elimination process, MCV and WE were removed to ensure that all remaining derivatives had minimal collinearity (VIF $\leq$ 3; Figure 5a). No flora variables (Set 2) exhibited significant pairwise correlation and all were retained (Figure 5b). No significant collinearity issues were detected between topography and flora variables (Set 3; Figure A2). The final topographic and flora variables used in modelling are presented in Figure 5.

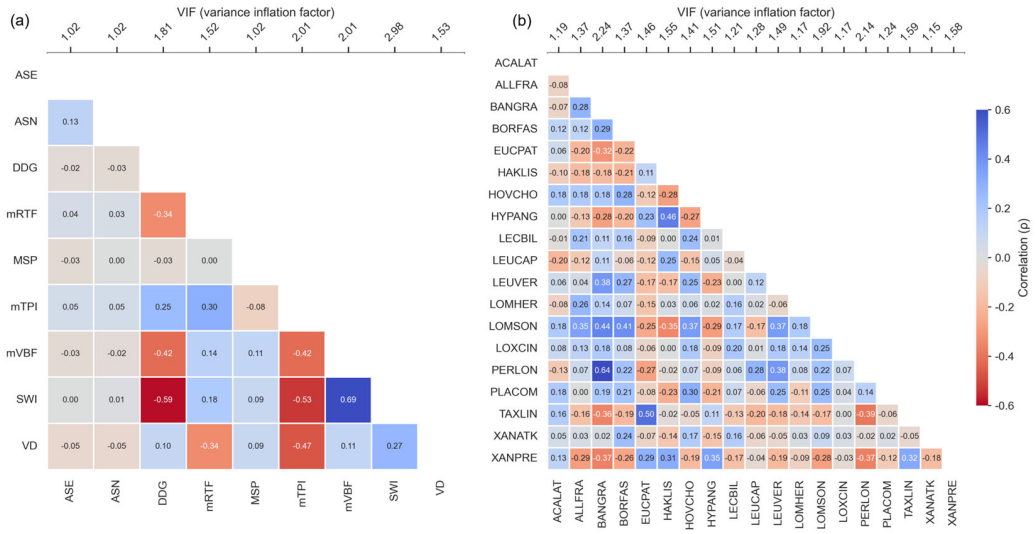

Figure 5. Pearson correlations and variance inflation factor (VIF) scores (top *x*-axis) of the final (**a**) topographic and (**b**) floristic variables used in species distribution models. Abbreviations for topographic and floristic variables are the same as those used in Table 2 and Figure 3, respectively.

3.2. Mineral Potential Modelling

The three sets of predictor variables were modelled separately to explore the strength of each in predicting bauxite. Considering the mean AUC of the heterogenous ensemble (HE) model (Figure 6) across all three sets, Set 3 yielded the highest AUC (0.88), followed by Set 2 (AUC: 0.85) and Set 1 (AUC: 0.82). The Wilcoxon–Mann–Whitney tests suggested that the mean model AUC of Set 3 (a combination of Sets 1 and 2) was significantly different to the other variable groups (Figure 6), indicating that model performance was significantly improved by combining topographic and floristic variables.

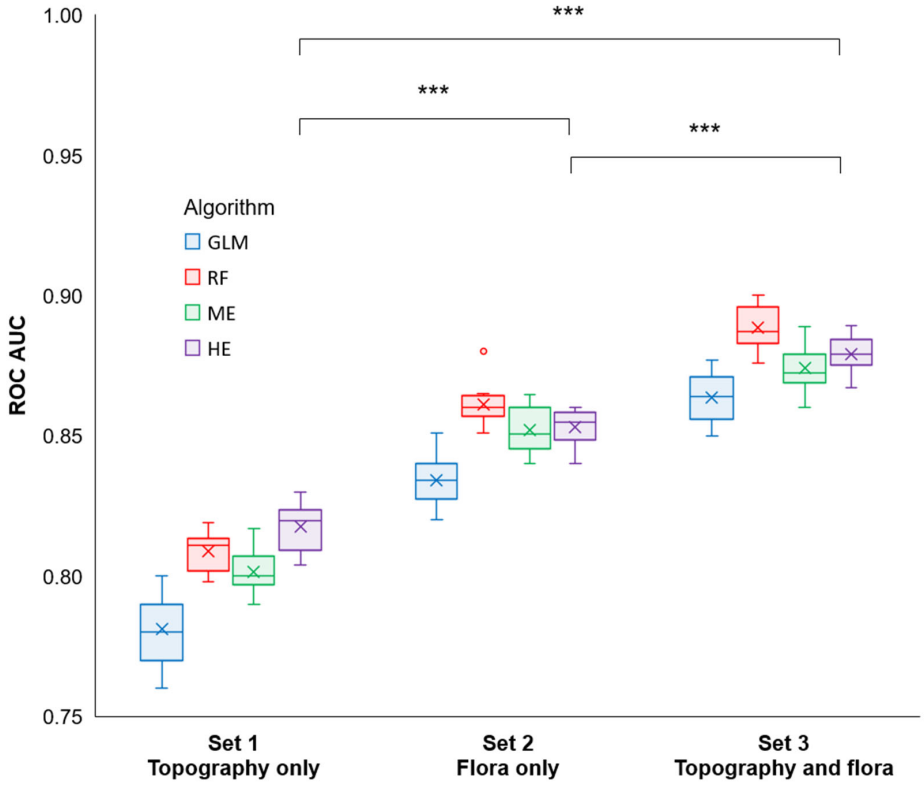

Figure 6. Analysis of the area under the curve (AUC) metric of the models generated for bauxite potential modelling. Three sets were tested, including topographic (Set 1) and floristic variables

(Set 2), as well as a combination of both (Set 3). Algorithms GLM, RF, and ME were used to build independent models as well as a heterogenous ensemble (HE) of all algorithms. The Wilcoxon–Mann–Whitney test was used to compare whether the mean ensemble model AUC of each variable set was significantly different. A significance level of 0.01 is represented as "***".

3.2.1. Variable Reduction and Model Optimisation

The maximum number of redundant predictor variables were removed without a significant ($p < 0.05$) impact on the model AUC using the stepwise DeLong comparison test (Table 3). With few exceptions, the minimal set of topographic (Table 3A), floristic (Table 3B), and combined variables (Table 3C) were consistently observed across final models. See Table A1 for an overview of all variables that were removed from the final models.

Table 3. Minimum set of variables and optimal AUC obtained using a stepwise DeLong comparison test to remove variables with a statistically insignificant impact on the model AUC. The DeLong test was undertaken separately for (A) topographic variables only (Set 1), (B) floristic variables only (Set 2), and (C) topography and flora variables combined (Set 3). The DeLong test was applied to the homogenous (GLM, RF, and ME) and the heterogenous ensemble (HE) models for each set of variables. Abbreviations for topographic and floristic variables are the same as those used in Table 2 and Figure 3, respectively.

	Set		GLM	RF	ME	HE
A.	Set 1 Topography only	Final variables	DDG mTPI SWI VD	mRTF MSP mTPI SWI VD	DDG mRTF MSP mTPI SWI VD	DDG mRTF MSP mTPI SWI VD
		AUC	0.78	0.81	0.80	0.82
B.	Set 2 Flora only	Final variables	BANGRA EUCPAT HAKLIS HYPANG LEUVER LOMSON PERLON PLACOM XANPRE	BANGRA HAKLIS HYPANG LEUVER LOMSON PERLON TAXLIN XANPRE	BANGRA HAKLIS HOVCHO HYPANG LEUVER LOMSON PLACOM TAXLIN XANPRE	BANGRA EUCPAT HAKLIS HOVCHO HYPANG LEUVER LOMSON PERLON PLACOM TAXLIN XANPRE
		AUC	0.83	0.86	0.85	0.85
C.	Set 3 Topography and flora	Final variables	BANGRA DDG HAKLIS HYPANG LEUVER LOMSON mTPI PERLON SWI VD XANPRE	BANGRA HAKLIS HYPANG LEUVER mRTF mTPI PERLON SWI TAXLIN VD XANPRE	BANGRA DDG HAKLIS HOVCHO HYPANG LEUVER LOMSON MSP mTPI PLACOM SWI VD XANPRE	BANGRA DDG HAKLIS HOVCHO HYPANG LEUVER LOMSON mRTF MSP mTPI PERLON PLACOM SWI TAXLIN VD XANPRE
		AUC	0.86	0.89	0.87	0.88

Mean variable importance was obtained from the final optimised models and is presented in Figure 7. SAGA wetness index (SWI), valley depth (VD) and multiscale topographic position (mTPI) were most important when modelling bauxite using topography only (Set 1; Figure 7a), with each contributing c. 48%, c. 27% and c. 17% to the final model, respectively. Furthermore, *Banksia grandis* (BANGRA; c. 35%), *Xanthorrea preissii* (XANPRE; c. 23%), *Hypocalymma angustifolium* (HYPANG; c. 20%) and *Hakea lissocarpha* (HAKLIS; c. 14%) were amongst the most important plant species identified from the flora-only models (Set 2; Figure 7b). These same variables maintained their relative importance within the combined variable model (Set 3; Figure 7c), with *B. grandis*, SWI, VD and *X. preissii* determined most important.

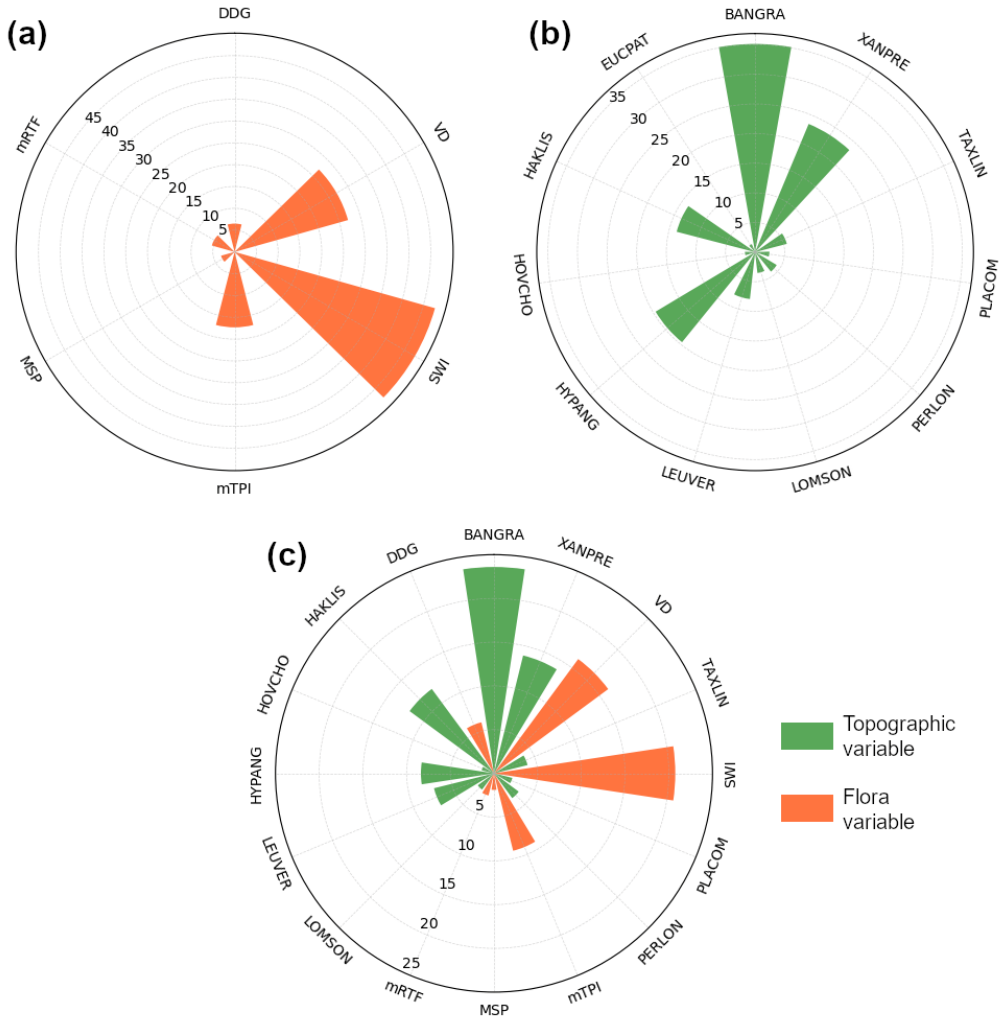

Figure 7. Mean variable importance (represented as a percentage) obtained from the final optimised bauxite potential models when using (**a**) Set 1 (topographic variables only), (**b**) Set 2 (flora variables only) and (**c**) Set 3 (all topographic and floristic variables combined). The bars represent individual variables and their mean importance within each model set. A bar closer to the outer radial axis has higher variable importance than a bar close to the chart centroid. Orange and green bar colours represent topographic and flora variables, respectively.

3.2.2. Variable Response Curves

Response curves for the seventeen optimal predictor variables are shown in Figure 8. Topographies with low to moderate amounts of soil moisture, rather than waterlogged areas, were found to be more suitable for bauxite based on the SAGA wetness curve (SWI; Figure 8a). Additionally, topographies with lower valley depths (c. < 30 m; Figure 8b) were also found to be most suitable, suggesting that bauxite was more likely in upland terrain away from valleys.

The multiscale topographic position (mTPI; Figure 8c) peaked at a value of 1, suggesting that lower, subdued hills are most suitable. *Banksia grandis* (BANGRA; Figure 8d) exhibited a strong positive relationship with bauxite; as *B. grandis* occurrence increased in the region, bauxite occurrence became more likely. Other notable positive, albeit weaker, relationships with bauxite were observed for *Leucopogon verticillatus* (LEUVER; Figure 8e), *Lomandra sonderi* (LOMSON; Figure 8f), *Persoonia longifolia* (PERLON; Figure 8g), *Platysace commutata* (PLACOM; Figure 8h) and *Hovea chorizemifolia* (HOVCHO; Figure 8i). In contrast, bauxitised ground was present in areas where the species *Hakea lissocarpha* (HAKLIS; Figure 8j), *Hypocalymma angustifolium* (HYPANG; Figure 8k) and *Xanthorrhoea preissii* (XANPRE; Figure 8l) were less likely to occur or were absent. This pattern was also true for *Taxandria linearoflia* (TAXLIN; Figure 8m) and *Eucalyptus patens* (EUCPAT; Figure 8n), albeit with less pronounced response curves.

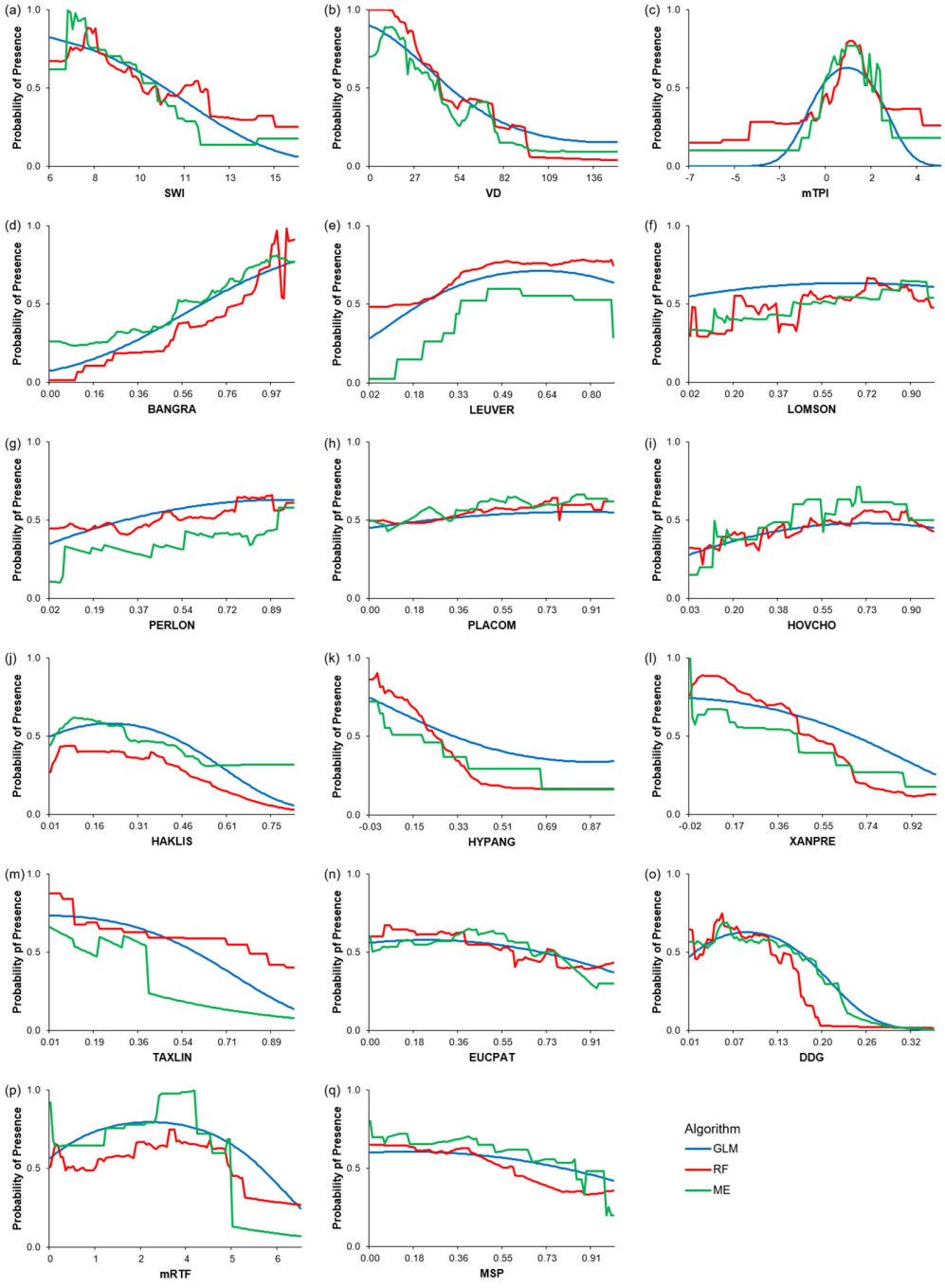

Figure 8. Response curves characterising the relationship between probability of bauxite presence and each variable (**a**–**q**). Curves represent a model created by each algorithm independently using

only one of each of the 17 variables. For example, (**a**) presents the response of bauxite probability to SAGA wetness index (SWI) values, while (**q**) shows the response when the mid-slope position (MSP) variable is used. Abbreviations for topographic and floristic variables are the same as those used in Table 2 and Figure 3, respectively. Blue, red and green colours represent curves from the GLM, RF and ME algorithms, respectively.

The final bauxite potential maps obtained from the heterogenous ensemble model are provided in Figure 9 and include maps based on Set 1 (topography only; Figure 9a), Set 2 (flora only; Figure 9b) and Set 3 (combined; Figure 9c).

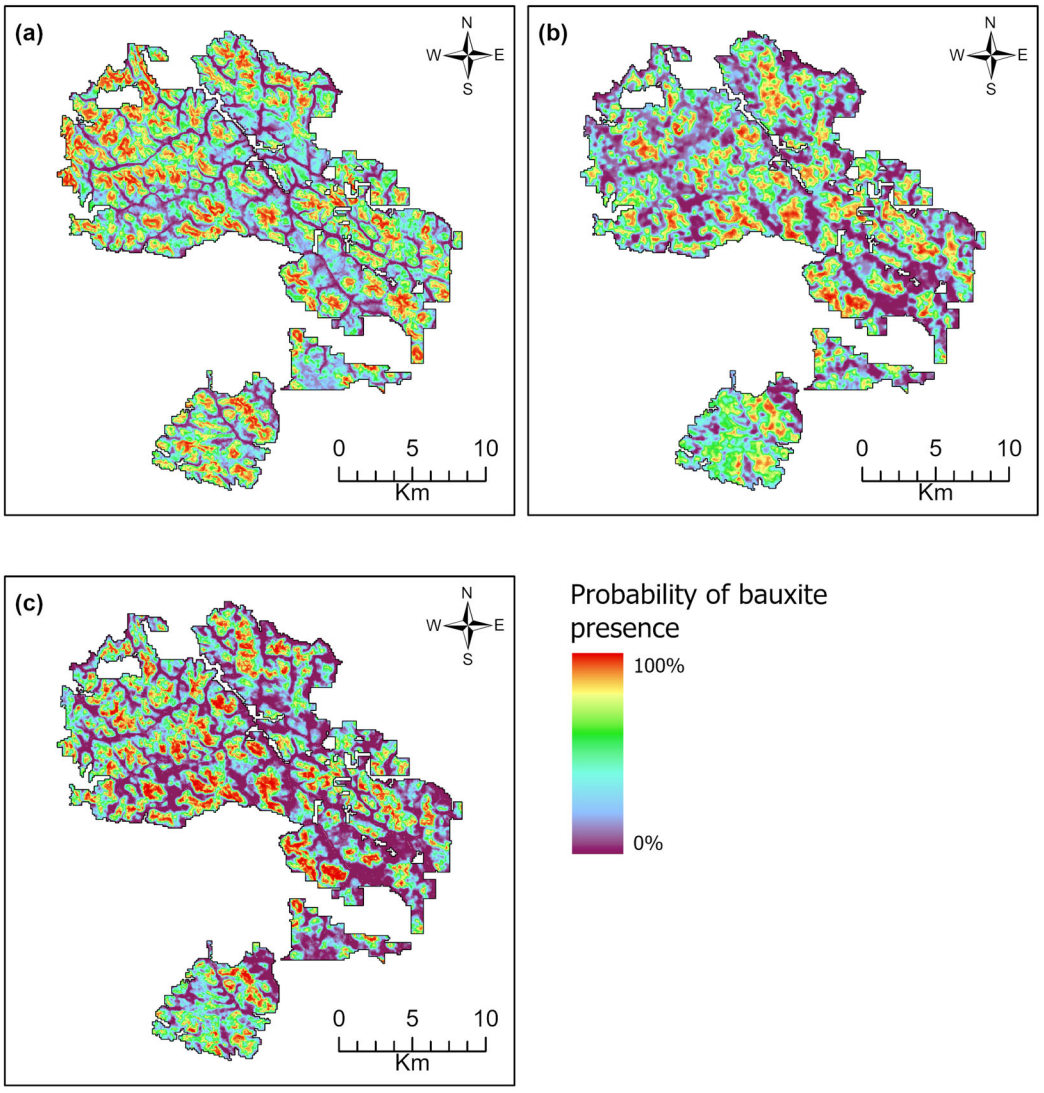

Figure 9. Projected potential maps of bauxite occurrence based on models comprising (**a**) Set 1—topographic derivatives only; (**b**) Set 2—flora species only; and (**c**) Set 3—all selected variables.

4. Discussion

As the global demand for mineral resources has accelerated in recent years [98], innovative modelling approaches are required to assist in their discovery. A particular advantage of mineral potential models is that they constitute an evidence-based targeting tool that can be easily updated with new and diverse evidence [41]. However, despite the potential of exploiting in situ plant occurrence to detect subsurface minerals, no studies have utilised this information in mineral modelling. We found that including geobotanical evidence introduced new, non-redundant information into our models based only on

derivatives of topology and on improved discrimination in presence–absence records of bauxite.

4.1. Model Variables

4.1.1. Indicator Plant Species

This study utilised a rich database of floristic surveys to explore this potential. Unlike traditional geobotanical methods, which rely on in situ qualitative surveys for mineral-related plants known a priori, our approach combines plant and mineral occurrence data with machine learning to statistically relate plants and minerals for the purpose of identifying new indicator plants and predicting the probability of mineral occurrence in unexplored landscapes. We determined *Banksia grandis* to have a significant association with bauxite presence (Figures 7 and 8). *B. grandis* is a dominant midstorey shrub or tree occurring at heights of up to 10 m in the region [99]. Though it is widespread, some studies suggest an association with bauxite substrate. *B. grandis* tends to grow on lateritic gravels [100] and is statistically correlated with the mid-slopes of bauxite-rich upland hills (e.g., [101,102]). Therefore, *B. grandis* distribution may act as a proxy variable of topographic control in our models. Nonetheless, the Banksia taxon has been identified as a hyperaccumulator of aluminium [103], and anomalous traces have been found in its leaves in the same region [104], which Lambers et al. [105] attributes to its detoxification mechanisms. This indicates that *B. grandis* is likely to at least have a resistance to soils with high aluminium concentrations, if not a preference for them. Biogeochemical analysis of leaf tissue is recommended to confirm this [106].

A further five taxa were associated with bauxite presence. The most notable were *Leucopogon verticillatus*, *Persoonia longifolia* and *Hovea chorizemifolia*, all of which frequently occur on the gravelly undulating hills characteristic of deposits in the region [101]. The relatively low importance of *L. verticillatus* and *H. chorizemifolia* in our models (Figure 7), especially compared to *B. grandis*, may be explained by their aversion to the drier sandy gravels common at deposits (Figure 2a) and their tendency to occur on upper hill slopes where bauxite formation is suboptimal [53,55]. Likewise, the infrequency of *H. chorizemifolia* observations in our dataset (Figure 3) may have also contributed to the taxon's low model importance. The remaining taxa *Lomandra sonderi* and *Platysace compressa* were very low in importance in our models (Figure 7) and produced very weak positive relationships with bauxite potential according to our response curves (Figure 8).

Five taxa were found to be associated with bauxite absence. Four of these (*Taxandria linearifolia*, *Hypocalymma angustifolium*, *Hakea lissocarpha* and *Eucalyptus patens)* occur on the edges of swamps and valleys or on lower hill slopes [101,107], which were situated away from known locations of bauxite. *Xanthorrhoea preissii*, a tree-like monocotyledon that dominates the forest understorey [108], also tended to occur more commonly away from bauxite deposits. This is most likely because its roots struggle to reach the moist clays beneath the duricrust zone (Figure 2), reducing survivability during drought [109,110].

4.1.2. Topographic Variables

We found three topographic variables that were strong predictors of bauxite (Figure 7). The most important was topographic wetness (SWI), which quantifies variation in soil wetness associated with runoff [111]. In the Darling Range, economic bauxite forms on hillsides where water is well drained. The movement of water downhill promotes bauxitisation by removing inhibiting solutions (e.g., silica) from weathering areas [112]. Ore grade declines further downhill as slope gradients depreciate, and drainage accumulates and stagnates [58]. The response curve for the SWI variable suggested that bauxite was situated in relatively dry locations of the catchment (Figure 8a). In subdued landscapes, lower topographic wetness may represent hillsides with appreciable slopes or hill crests [113].

Valley depth (VD) was also a strong bauxite predictor (Figure 7). In the region, deposits are frequently dissected by either shallow or deeply incised valleys [55]. Bauxite is absent in valleys, as laterite is highly eroded, and soil conditions inhibit weathering [57].

The valley depth variable clearly distinguished broad valley areas from upper geomorphology (Figure 9a), and deposits tended to occur away from valleys (Figure 8b). Additional information about the relative positions of bauxite on hills was incorporated via the multiscale topographic position index (mTPI). The mTPI showed that most bauxite occurred where mTPI ≈ 0.5–1.5, which describes the middle to upper positions of hills (Figure 2a), but below hill crests [114]. This corroborates anecdotal evidence from field workers in the region [61,115,116] and findings relating topographic position indices to comparable lateritic deposits [117].

4.2. Mineral Potential Modelling

To gauge the potential of topographic variables and plant taxa for modelling bauxite individually and collectively, we modelled bauxite using three variable sets (i.e., topo-only, flora-only and both). Almost all models obtained a mean AUC higher than 0.8, indicating a good level of discrimination between presence and absence in our data [118]. Flora-only models (0.83–0.86) outperformed topo-only models (0.78–0.82). While the topographic variables accurately captured overland drainage processes and deposit position in our case study, these metrics are less capable of representing subsurface soil conditions in low-relief terrain [119,120]. It is likely that plant distribution provided indirect information not only on topography [121] but also on subsurface soil chemistry [122] and mineralisation [123].

In the studied region, ore is restricted to lateritic soil [61]. Tall trees promote lateritic weathering by fixing soils, regulating water percolation and runoff, and reducing soil acidity in the substrate [55]. As no significant pairwise correlations were observed between the 19 candidate taxa (Figure 5b), each species reflected relatively different outcomes of the bauxite formation process in terms of the rootzone soil properties that vary across the landscape. As such, we suspect that plant species distributions, particularly when used in combination, incorporated unique information about these local soil processes, which the terrain metrics could not. Additionally, the SRTM DEM used may exhibit increased vertical error in forested regions [124], potentially increasing uncertainty in our topo-only model. Regardless, the combination of both plant distributions and topographic variables showed the best results in model performance, and the inclusion of terrain metrics improved the clarity of the projected spatial patterns of bauxite deposits, particularly in lower valley areas (Figure 9).

Akin to not relying solely on one opinion, modern ensemble techniques merge multiple model algorithms together to reduce the generalisation error of the prediction. Several recent studies found that heterogenous stacking ensembles improved mineral prediction accuracy when compared to singular models (e.g., [41,48,125]). Our findings contradict these, as we found that GLM-RF-ME ensembles generally performed worse than homogenous RF models, and only marginally better than ME models (Figure 6). Ensemble techniques (such as biomod) are prominent in the recent species distribution modelling (SDM) literature for their potential to improve predictive ability [44,126]. However, some have suggested that these techniques do not necessarily produce optimal models, may elevate overfitting, and add unnecessary complexity [127,128]. Our findings align with Hao et al. [129] and Valavi et al. [130], who both compared SDM techniques and found that heterogenous biomod ensembles performed no better (and occasionally worse) than standard models when trained with default biomod parameters.

4.3. Model Limitations and Recommendations

An inherent source of uncertainty in mineral potential modelling stems from the general unavailability of exploration data, leading to the omission of key mineralisation evidence [131]. While our models incorporate vital topographic factors, evidence such as surficial geology and geophysics geodata often applied in prospecting [132] could not be sourced. Most known bauxite deposits are restricted to lateritic soils overlying aluminosilicate rocks [133]. While several studies have improved bauxite targeting by isolating these types on regolith maps (e.g., [134,135]), local-scale geological mapping

(e.g., [136]) is unavailable in our region. In these cases, multispectral satellite imagery can help determine laterite extent [137,138], but these become highly unreliable in dense forest canopies [139]. Our ability to include radiometric and gravity data, which could help distinguish granite parent rocks [140], was also limited due to their post-mining capture (i.e., earliest available is from 2007; [141]). Despite these limitations, we managed to improve our models by explaining some of these missing factors using proxies, such as local soil distribution according to plant occurrence. These findings reinforce recent suggestions that mineral modelling could benefit from a multidisciplinary data approach in the machine learning era [15].

Another potential limitation of our geobotanical modelling approach is the need for in situ plant observations from underexplored regions. Admittedly, we used a well-sampled and far-reaching floristic plot geodatabase [65] to create our species probability maps. It is unlikely that comparable databases are available for public use, although we expect that suitable alternatives may exist due to regulatory pre-impact surveys. Regardless, SDM offers a possible solution when plant data are limited. Ecologists have long used SDM to extrapolate plant habitat in underexplored landscapes, even when species observations are limited (e.g., [142,143]). Therefore, plant occurrences taken from well-surveyed areas could be used to predict species probability in underexplored landscapes, and these outputs could be applied as evidence in mineral potential models, especially when indicator species are known a priori.

5. Conclusions

Our results show that taking an inductive approach to floristic survey databases can reveal previously unknown associations between plant species and mineral targets. This is highly transferrable to other targets and a modern alternative for discovering plants as indicators for a wide range of purposes. In addition, where floristic surveys already exist, the process is extremely cost-effective and value-adding, and relative to other methods of survey and exploration, it has very low impact on the environment. We demonstrate that topographic variables representative of topographic wetness, position and valley depth are useful for capturing complex formation controls of bauxite deposits in south-western Australia. The addition of floristic surveys improved the accuracy of our model by providing unique evidence about the overlying botanical life that either avoids, is tolerant to or accumulates minerals in bauxite-rich soils. Of the several statistical and machine learning approaches utilised, the random forest model was found to discriminate between known bauxite presence and absence locations (AUC = 0.89). Unlike recent studies, we found that heterogenous ensemble methods did not significantly improve model accuracy, and the best approach was identified using random forest models. As opposed to more invasive exploration techniques such as drilling, both topographic variables and floristic surveys have no impact on the surrounding environment. These data can be valuable inclusions in future applications of mineral potential modelling.

Author Contributions: Conceptualization, T.P.R., L.T. and G.W.-J.; methodology, L.T. and T.P.R.; software, L.T.; validation, L.T.; formal analysis, L.T.; investigation, L.T.; resources, A.G. and L.T.; data curation, L.T. and S.L.; writing—original draft preparation, L.T.; writing—review and editing, T.P.R., G.W.-J., A.G., S.L. and L.T.; visualisation, L.T.; supervision, T.P.R. and G.W.-J.; project administration, L.T. and T.P.R.; funding acquisition, L.T., T.P.R. and G.W.-J. All authors have read and agreed to the published version of the manuscript.

Funding: This research was supported by the Australian Federal Government via stipend funding provided by the Research Training Program (RTP; formally the Australian Postgraduate Award scholarship).

Data Availability Statement: The floristic plot database used in this article is not readily available as the data are part of an ongoing study. Additionally, the bauxite drillhole dataset is not readily available due to its commercial sensitivity. Other datasets are available on request from the corresponding author.

Acknowledgments: The authors wish to thank the three anonymous reviewers for their helpful feedback during the peer-review process.

Conflicts of Interest: Andrew Grigg is employed at the company Alcoa of Australia. The remaining authors declare that the research was conducted in the absence of any commercial or financial relationships that could be construed as potential conflicts of interest.

Appendix A

Table A1. Root-mean-square error (RMSE) obtained from the disjunctive kriging process. Disjunctive kriging was used to interpolate binary species occurrence (i.e., 0, 1 or presence/absence) geolocations into continuous probability surfaces.

Species Name	Abbreviation	Root-Mean-Square Error
Acacia lateriticola	ACALAT	0.165
Allocasuarina fraseriana	ALLFRA	0.216
Banksia grandis	BANGRA	0.281
Boronia fastigiata	BORFAS	0.341
Eucalyptus patens	EUCPAT	0.119
Hakea lissocarpha	HAKLIS	0.166
Hovea chorizemifolia	HOVCHO	0.268
Hypocalymma angustifolium	HYPANG	0.175
Lechenaultia biloba	LECBIL	0.232
Leucopogon capitellatus	LEUCAP	0.254
Leucopogon verticillatus	LEUVER	0.241
Lomandra hermaphrodita	LOMHER	0.234
Lomandra sonderi	LOMSON	0.309
Loxocarya cinerea	LOXCIN	0.167
Persoonia longifolia	PERLON	0.299
Platysace commutata	PLACOM	0.171
Taxandria linearifolia	TAXLIN	0.093
Xanthorrhoea preissii	XANPRE	0.259
Xanthosia atkinsoniana	XANATK	0.166
Mean		0.219

Appendix B

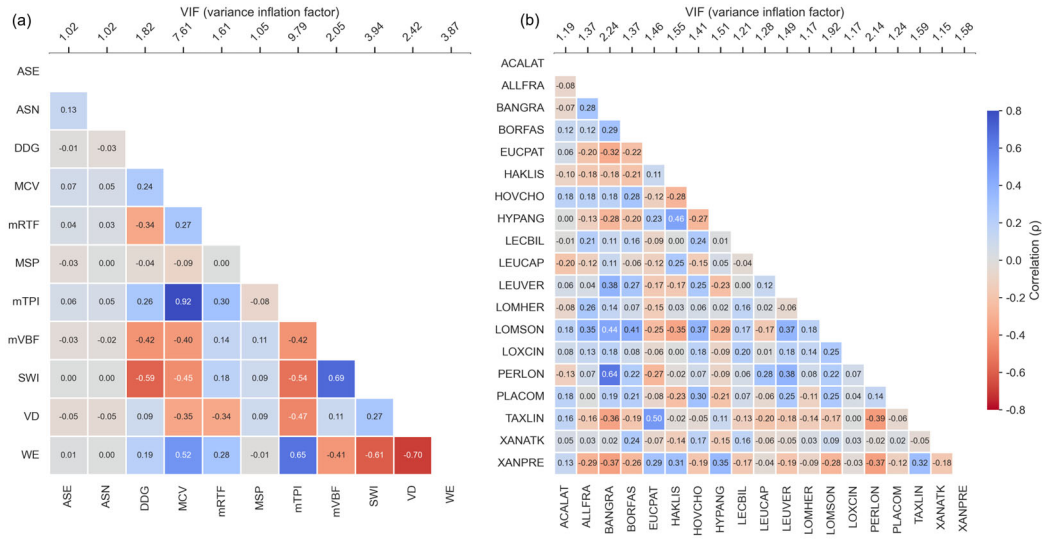

Figure A1. Pearson correlations and variance inflation factor (VIF) scores (top *x*-axis) of all initial (**a**) topographic and (**b**) floristic variables used in species distribution models.

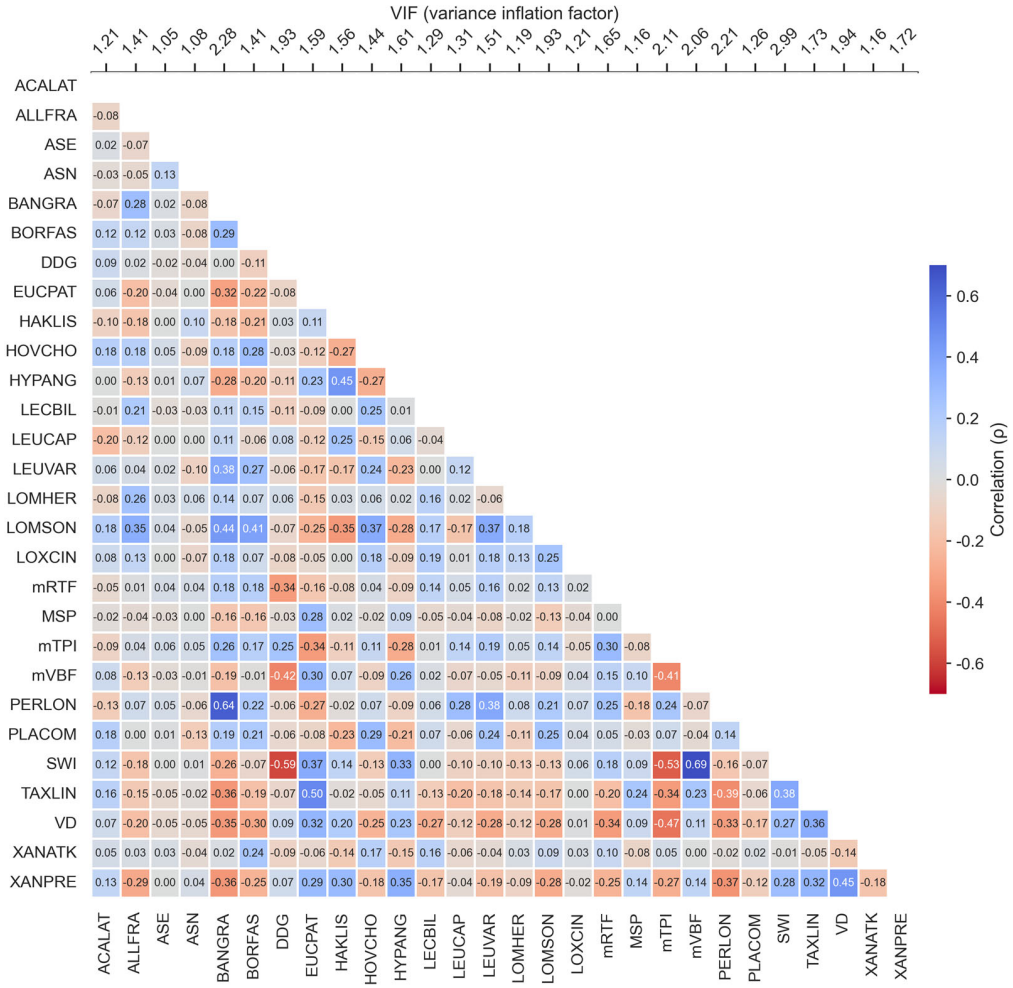

Figure A2. Pearson correlations and variance inflation factor (VIF) scores (top *x*-axis) of the final topographic and floristic variables used in species distribution models combined.

Appendix C

Table A2. Variables that were excluded from the final models during the stepwise DeLong comparison test. These variables had a statistically insignificant impact on model AUC. The DeLong test was undertaken separately for (A) topographic variables only (Set 1), (B) floristic variables only (Set 2), and (C) topography and flora variables combined (Set 3). The DeLong test was applied to the homogenous (GLM, RF and ME) and the heterogenous ensemble (HE) models for each set of variables.

Set			GLM	RF	ME	HE
A.	Set 1 Topography only	Excluded variables	ASE ASN mRTF MSP mVBF	ASE ASN DDG	ASE ASN mVBF	ASE ASN mVBF
B.	Set 2 Flora only	Excluded variables	ACALAT ALLFRA BORFAS HOVCHO LECBIL LEUCAP LOMHER LOXCIN TAXLIN XANATK	ACALAT ALLFRA BORFAS EUCPAT HOVCHO LECBIL LEUCAP LOMHER LOXCIN PLACOM XANATK	ACALAT ALLFRA BORFAS EUCPAT LECBIL LEUCAP LOMHER LOXCIN PERLON XANATK	ACALAT ALLFRA BORFAS LECBIL LEUCAP LOMHER LOXCIN XANATK

Table A2. *Cont.*

Set			GLM	RF	ME	HE
C.	Set 3 Topography and flora	Excluded variables	ACALAT ALLFRA ASE ASN BORFAS EUCPAT HOVCHO LECBIL LEUCAP LOMHER LOXCIN mRTF MSP mVBF PLACOM TAXLIN XANATK	ACALAT ALLFRA ASE ASN BORFAS DDG EUCPAT HOVCHO LECBIL LEUCAP LOMHER LOMSON LOXCIN MSP mVBF PLACOM XANATK	ACALAT ALLFRA ASE ASN BORFAS EUCPAT LECBIL LEUCAP LOMHER LOXCIN mRTF mVBF PERLON TAXLIN XANATK	ACALAT ALLFRA ASE ASN BORFAS EUCPAT LECBIL LEUCAP LOMHER LOXCIN mVBF VD XANPRE

References

1. Brooks, R. Indicator Plants for Mineral Prospecting—A Critique. *J. Geochem. Explor.* **1979**, *12*, 67–78. [CrossRef]
2. Brooks, R.R. *Geobotanical Prospecting*; Encyclopedia of Earth Science; Springer: Boston, MA, USA, 1988; ISBN 978-0-387-30844-9.
3. Sampson, A.W. Plant Indicators—Concept and Status. *Bot. Rev.* **1939**, *5*, 155–206. [CrossRef]
4. Cannon, H.L. Botanical Prospecting for Ore Deposits: How Plant Chemistry Is Being Used to Aid the Geologist in His Search for Metals at Home and Abroad. *Science* **1960**, *132*, 591–598. [CrossRef] [PubMed]
5. Boyd, R.S. Ecology of Metal Hyperaccumulation. *New Phytol.* **2004**, *16*, 563–567. [CrossRef]
6. Schreiber, H.D.; Jones, A.H.; Lariviere, C.M.; Mayhew, K.M.; Cain, J.B. Role of Aluminum in Red-to-Blue Color Changes in Hydrangea Macrophylla Sepals. *Biometals* **2011**, *24*, 1005–1015. [CrossRef]
7. Cannon, H.L. The Use of Plant Indicators in Ground Water Surveys, Geologic Mapping, and Mineral Prospecting. *Taxon* **1971**, *20*, 227–256. [CrossRef]
8. Odhiambo, B.D. The Place of Geobotany in Geology. *Int. J. Geobot. Res* **2016**, *6*, 27–36.
9. Knox-Robinson, C.; Wyborn, L. Towards a Holistic Exploration Strategy: Using Geographic Information Systems as a Tool to Enhance Exploration. *Aust. J. Earth Sci.* **1997**, *44*, 453–463. [CrossRef]
10. Carranza, E.J.M. *Geochemical Anomaly and Mineral Prospectivity Mapping in GIS*; Elsevier: Amsterdam, The Netherlands, 2008; ISBN 0-08-093031-X.
11. Bonham-Carter, G. *Geographic Information Systems for Geoscientists: Modelling with GIS*; Elsevier: Amsterdam, The Netherlands, 1994; ISBN 0-08-042420-1.
12. Harris, J.; Wilkinson, L.; Grunsky, E.; Heather, K.; Ayer, J. Techniques for Analysis and Visualization of Lithoge-ochemical Data with Applications to the Swayze Greenstone Belt, Ontario. *J. Geochem. Explor.* **1999**, *67*, 301–334. [CrossRef]
13. An, P.; Moon, W.; Rencz, A. Application of Fuzzy Set Theory for Integration of Geological, Geophysical and Re-mote Sensing Data. *Can. J. Explor. Geophys.* **1991**, *27*, 1–11.
14. An, P.; Moon, W.; Bonham-Carter, G. Uncertainty Management in Integration of Exploration Data Using the Be-lief Function. *Nonrenewable Resour.* **1994**, *3*, 60–71. [CrossRef]
15. Yousefi, M.; Carranza, E.J.M.; Kreuzer, O.P.; Nykänen, V.; Hronsky, J.M.; Mihalasky, M.J. Data Analysis Methods for Prospectivity Modelling as Applied to Mineral Exploration Targeting: State-of-the-Art and Outlook. *J. Geochem. Explor.* **2021**, *229*, 106839. [CrossRef]
16. Porwal, A.; Carranza, E.J.M.; Hale, M. Bayesian Network Classifiers for Mineral Potential Mapping. *Comput. Geosci.* **2006**, *32*, 1–16. [CrossRef]
17. Chung, C.; Agterberg, F. Regression Models for Estimating Mineral Resources from Geological Map Data. *J. Int. Assoc. Math. Geol.* **1980**, *12*, 473–488. [CrossRef]
18. Cheng, Q.; Agterberg, F. Fuzzy Weights of Evidence Method and Its Application in Mineral Potential Mapping. *Nat. Resour. Res.* **1999**, *8*, 27–35. [CrossRef]
19. Rodriguez-Galiano, V.; Sanchez-Castillo, M.; Chica-Olmo, M.; Chica-Rivas, M. Machine Learning Predictive Models for Mineral Prospectivity: An Evaluation of Neural Networks, Random Forest, Regression Trees and Support Vector Machines. *Ore Geol. Rev.* **2015**, *71*, 804–818. [CrossRef]
20. Sun, T.; Chen, F.; Zhong, L.; Liu, W.; Wang, Y. GIS-Based Mineral Prospectivity Mapping Using Machine Learn-ing Methods: A Case Study from Tongling Ore District, Eastern China. *Ore Geol. Rev.* **2019**, *109*, 26–49. [CrossRef]
21. Liu, Y.; Zhou, K.; Xia, Q. A MaxEnt Model for Mineral Prospectivity Mapping. *Nat. Resour. Res.* **2018**, *27*, 299–313. [CrossRef]
22. Porwal, A.; Carranza, E.; Hale, M. Artificial Neural Networks for Mineral-Potential Mapping: A Case Study from Aravalli Province, Western India. *Nat. Resour. Res.* **2003**, *12*, 155–171. [CrossRef]

23. Carranza, E.J.M.; Laborte, A.G. Random Forest Predictive Modeling of Mineral Prospectivity with Small Number of Prospects and Data with Missing Values in Abra (Philippines). *Comput. Geosci.* **2015**, *74*, 60–70. [CrossRef]
24. Zuo, R.; Carranza, E.J.M. Support Vector Machine: A Tool for Mapping Mineral Prospectivity. *Comput. Geo-Sci.* **2011**, *37*, 1967–1975. [CrossRef]
25. Dumakor-Dupey, N.K.; Arya, S. Machine Learning—A Review of Applications in Mineral Resource Estimation. *Energies* **2021**, *14*, 4079. [CrossRef]
26. Rodriguez-Galiano, V.; Chica-Olmo, M.; Chica-Rivas, M. Predictive Modelling of Gold Potential with the Integra-tion of Multisource Information Based on Random Forest: A Case Study on the Rodalquilar Area, Southern Spain. *Int. J. Geogr. Inf. Sci.* **2014**, *28*, 1336–1354. [CrossRef]
27. Zhang, D.; Agterberg, F.; Cheng, Q.; Zuo, R. A Comparison of Modified Fuzzy Weights of Evidence, Fuzzy Weights of Evidence, and Logistic Regression for Mapping Mineral Prospectivity. *Math. Geosci.* **2014**, *46*, 869–885. [CrossRef]
28. Collins, W.; Chang, S.-H.; Raines, G.L.; Canney, F.; Ashley, R. Airborne Biogeophysical Mapping of Hidden Min-eral Deposits. *Econ. Geol.* **1983**, *78*, 737–749. [CrossRef]
29. De Almeida, T.I.R.; De Souza Filho, C.R.; Juliani, C.; Branco, F.C. *Application of Remote Sensing to Geobotany to Detect Hydrothermal Alteration Facies in Epithermal High-Sulfidation Gold Deposits in the Amazon Region*; Society of Economic Geologists, Inc.: Littleton, CO, USA, 2009.
30. Hede, A.N.H.; Koike, K.; Kashiwaya, K.; Sakurai, S.; Yamada, R.; Singer, D.A. How Can Satellite Imagery Be Used for Mineral Exploration in Thick Vegetation Areas? *Geochem. Geophys. Geosystems* **2017**, *18*, 584–596. [CrossRef]
31. Paradella, W.; Da Silva, M.; Rosa, N. de A. A Geobotanical Approach to the Tropical Rain Forest Environment of the Carajás Mineral Province (Amazon Region, Brazil), Based on Digital TM-Landsat and DEM Data. *Int.-Al J. Remote Sens.* **1994**, *15*, 1633–1648. [CrossRef]
32. Mahmood, T.H.; Hasan, K.; Akhter, S.H. Lithologic Mapping of a Forested Montane Terrain from Landsat 5 TM Image. *Geocarto Int.* **2019**, *34*, 750–768. [CrossRef]
33. Ibanez, D.M.; Almeida-Filho, R.; Miranda, F.P. Analysis of SRTM Data as an Aid to Hydrocarbon Exploration in a Frontier Area of the Amazonas Sedimentary Basin, Northern Brazil. *Mar. Pet. Geol.* **2016**, *73*, 528–538. [CrossRef]
34. Carranza, E.J.M.; Mangaoang, J.C.; Hale, M. Application of Mineral Exploration Models and GIS to Generate Mineral Potential Maps as Input for Optimum Land-Use Planning in the Philippines. *Nat. Resour. Res.* **1999**, *8*, 165–173. [CrossRef]
35. Albrecht, T.; González-Álvarez, I.; Klump, J. Using Machine Learning to Map Western Australian Landscapes for Mineral Exploration. *ISPRS Int. J. Geo-Inf.* **2021**, *10*, 459. [CrossRef]
36. Hung, L.; Batelaan, O.; De Smedt, F. *Lineament Extraction and Analysis, Comparison of LANDSAT ETM and ASTER Imagery. Case Study: Suoimuoi Tropical Karst Catchment, Vietnam*; SPIE: Bellingham, WA, USA, 2005; Volume 5983, pp. 182–193.
37. Khalifani, F.M.; Bahroudi, A.; Aliyari, F.; Abedi, M.; Yousefi, M.; Mohammadpour, M. Generation of an Efficient Structural Evidence Layer for Mineral Exploration Targeting. *J. Afr. Earth Sci.* **2019**, *160*, 103609. [CrossRef]
38. Wang, H.; Yuan, Z.; Cheng, Q.; Zhang, S.; Sadeghi, B. Geochemical Anomaly Definition Using Stream Sediments Landscape Modeling. *Ore Geol. Rev.* **2022**, *142*, 104715. [CrossRef]
39. Arpit, D.; Wang, H.; Zhou, Y.; Xiong, C. Ensemble of Averages: Improving Model Selection and Boosting Perfor-mance in Domain Generalization. *Adv. Neural Inf. Process. Syst.* **2022**, *35*, 8265–8277.
40. Araújo, M.B.; New, M. Ensemble Forecasting of Species Distributions. *Trends Ecol. Evol.* **2007**, *22*, 42–47. [CrossRef]
41. Wang, K.; Zheng, X.; Wang, G.; Liu, D.; Cui, N. A Multi-Model Ensemble Approach for Gold Mineral Prospectivi-ty Mapping: A Case Study on the Beishan Region, Western China. *Minerals* **2020**, *10*, 1126. [CrossRef]
42. Sagi, O.; Rokach, L. Ensemble Learning: A Survey. *Wiley Interdiscip. Rev. Data Min. Knowl. Discov.* **2018**, *8*, e1249. [CrossRef]
43. Dou, J.; Yunus, A.P.; Bui, D.T.; Merghadi, A.; Sahana, M.; Zhu, Z.; Chen, C.-W.; Han, Z.; Pham, B.T. Improved Landslide Assessment Using Support Vector Machine with Bagging, Boosting, and Stacking Ensemble Machine Learning Framework in a Mountainous Watershed, Japan. *Landslides* **2020**, *17*, 641–658. [CrossRef]
44. Marmion, M.; Parviainen, M.; Luoto, M.; Heikkinen, R.K.; Thuiller, W. Evaluation of Consensus Methods in Pre-dictive Species Distribution Modelling. *Divers. Distrib.* **2009**, *15*, 59–69. [CrossRef]
45. Dong, X.; Yu, Z.; Cao, W.; Shi, Y.; Ma, Q. A Survey on Ensemble Learning. *Front. Comput. Sci.* **2020**, *14*, 241–258. [CrossRef]
46. Grenouillet, G.; Buisson, L.; Casajus, N.; Lek, S. Ensemble Modelling of Species Distribution: The Effects of Geo-graphical and Environmental Ranges. *Ecography* **2011**, *34*, 9–17. [CrossRef]
47. Yin, J.; Li, N. Ensemble Learning Models with a Bayesian Optimization Algorithm for Mineral Prospectivity Mapping. *Ore Geol. Rev.* **2022**, *145*, 104916. [CrossRef]
48. Hajihosseinlou, M.; Maghsoudi, A.; Ghezelbash, R. Stacking: A Novel Data-Driven Ensemble Machine Learning Strategy for Prediction and Mapping of Pb-Zn Prospectivity in Varcheh District, West Iran. *Expert Syst. Appl.* **2024**, *237*, 121668. [CrossRef]
49. Hughes, A.; Britt, A.; Pheeney, J.; Summerfield, D.; Senior, A.; Hitchman, A.P.; Cross, A.; Sexton, M.; Colclough, H.; Hill, J. *Australia's Identified Mineral Resources 2022*; Geoscience Australia: Canberra, Australia, 2023; ISBN 1-922625-36-1.
50. Robinson, T.; Di Virgilio, G.; Temple-Smith, D.; Hesford, J.; Wardell-Johnson, G. Characterisation of Range Re-striction amongst the Rare Flora of Banded Ironstone Formation Ranges in Semiarid South-Western Australia. *Aust. J. Bot.* **2018**, *67*, 234–247. [CrossRef]

51. Churchward, H.; Dimmock, G. The Soils and Landforms of the Northern Jarrah Forest. *Jarrah For. A Complex Mediterr. Ecosyst.* **1989**, *13*, 13–21.
52. Gentilli, J. Climate of the Jarrah Forest. In *The Jarrah Forest: A Complex Mediterranean Ecosystem*; Springer: Berlin/Heidelberg, Germany, 1989; pp. 23–40.
53. Havel, J.J. *Site-Vegetation Mapping in the Northern Jarrah Forest (Darling Range). Definition of Site-Vegetation Types*; Forests Department: Perth, Australia, 1975; ISBN 978-0-7244-7407-3.
54. Luxton, S.; Wardell-Johnson, G.; Sparrow, A.; Robinson, T.; Trotter, L.; Grigg, A. Vegetation Classification in South-Western Australia's Mediterranean Jarrah Forest: New Data, Old Units, and a Conservation Conundrum. *Aust. J. Bot.* **2021**, *69*, 436–449. [CrossRef]
55. Hickman, A.H. *Bauxite Mineralization in the Darling Range, Western Australia*; Geological Survey of Western Australia: Perth, Australia, 1992; Volume 33, ISBN 0-7309-4472-7.
56. Anand, R.; Gilkes, R.; Roach, G. Geochemical and Mineralogical Characteristics of Bauxites, Darling Range, Western Australia. *Appl. Geochem.* **1991**, *6*, 233–248. [CrossRef]
57. Tomich, S.A. Bauxite in the Darling Range, Western Australia. *Proc. Australas. Inst. Min. Metall. Proc.* **1964**, *212*, 125–135.
58. Geidans, L. *Bauxitic Laterites of the South Western Part of Western Australia*; The Australasian Institute of Mining and Metallurgy: Carlton, Australia, 1973.
59. Croton, J.T.; Reed, A.J. Hydrology and Bauxite Mining on the Darling Plateau. *Restor. Ecol.* **2007**, *15*, S40–S47. [CrossRef]
60. Kew, G.; Gilkes, R.; Mathison, C. Nature and Origins of Granitic Regolith in Bauxite Mine Floors in the Darling Range, Western Australia. *Aust. J. Earth Sci.* **2008**, *55*, 473–492. [CrossRef]
61. Anand, R.R.; Paine, M. Regolith Geology of the Yilgarn Craton, Western Australia: Implications for Exploration. *Aust. J. Earth Sci.* **2002**, *49*, 3–162. [CrossRef]
62. Grigg, A.H. Hydrological Response to Bauxite Mining and Rehabilitation in the Jarrah Forest in South West Australia. *J. Hydrol. Reg. Stud.* **2017**, *12*, 150–164. [CrossRef]
63. ESRI ArcGIS Pro (Version 3.3.0). ESRI: Redlands, CA, USA, 2023. Available online: http://www.esri.com (accessed on 1 December 2023).
64. Steen, V.A.; Tingley, M.W.; Paton, P.W.; Elphick, C.S. Spatial Thinning and Class Balancing: Key Choices Lead to Variation in the Performance of Species Distribution Models with Citizen Science Data. *Methods Ecol. Evol.* **2021**, *12*, 216–226. [CrossRef]
65. Trotter, L.; Robinson, T.P.; Wardell-Johnson, G.; Grigg, A.; Luxton, S. FIMS: A Free and Open-Source Spatial Database System for Plant Observation and Mobile Data Collection. *Phytocoenologia* **2018**, *48*, 393. [CrossRef]
66. Greenwood, P.E.; Nikulin, M.S. A Guide to Chi-Squared Testing. John Wiley & Sons: Hoboken, NJ, USA, 1996; Volume 280, ISBN 0-471-55779-X.
67. Matheron, G. *A Simple Substitute for Conditional Expectation: The Disjunctive Kriging*; Springer: Berlin/Heidelberg, Germany, 1976; pp. 221–236.
68. Men, M.; Yu, Z.; Xu, H. Study on the Spatial Pattern of Rainfall Erosivity Based on Geostatistics in Hebei Province, China. *Front. Agric. China* **2008**, *2*, 281–289. [CrossRef]
69. Robinson, T.; Metternicht, G. Testing the Performance of Spatial Interpolation Techniques for Mapping Soil Prop-erties. *Comput. Electron. Agric.* **2006**, *50*, 97–108. [CrossRef]
70. Gallant, J.; Wilson, N.; Dowling, T.; Read, A.; Inskeep, C. SRTM-Derived 1 Second Digital Elevation Models Version 1.0. Geoscience Australia: Canberra, Australia, 2011. Available online: https://pid.geoscience.gov.au/dataset/ga/72759 (accessed on 1 December 2023).
71. Conrad, O.; Bechtel, B.; Bock, M.; Dietrich, H.; Fischer, E.; Gerlitz, L.; Wehberg, J.; Wichmann, V.; Böhner, J. System for Automated Geoscientific Analyses (SAGA) v. 2.1. 4. *Geosci. Model Dev.* **2015**, *8*, 1991–2007. [CrossRef]
72. Amatulli, G.; Domisch, S.; Tuanmu, M.-N.; Parmentier, B.; Ranipeta, A.; Malczyk, J.; Jetz, W. A Suite of Global, Cross-Scale Topographic Variables for Environmental and Biodiversity Modeling. *Sci. Data* **2018**, *5*, 180040. [CrossRef]
73. Minár, J.; Evans, I.S.; Jenčo, M. A Comprehensive System of Definitions of Land Surface (Topographic) Curvatures, with Implications for Their Application in Geoscience Modelling and Prediction. *Earth-Sci. Rev.* **2020**, *211*, 103414. [CrossRef]
74. Guisan, A.; Weiss, S.B.; Weiss, A.D. GLM versus CCA Spatial Modeling of Plant Species Distribution. *Plant Ecol.* **1999**, *143*, 107–122. [CrossRef]
75. Lindsay, J.B.; Cockburn, J.; Russell, H. An Integral Image Approach to Performing Multi-Scale Topographic Position Analysis. *Geomorphology* **2015**, *245*, 51–61. [CrossRef]
76. Schwager, P.; Berg, C. Remote Sensing Variables Improve Species Distribution Models for Alpine Plant Species. *Basic Appl. Ecol.* **2021**, *54*, 1–13. [CrossRef]
77. Hjerdt, K.; McDonnell, J.; Seibert, J.; Rodhe, A. A New Topographic Index to Quantify Downslope Controls on Local Drainage. *Water Resour. Res.* **2004**, *40*, W05602. [CrossRef]
78. Böhner, J.; Selige, T. Spatial Prediction of Soil Attributes Using Terrain Analysis and Climate Regionalisation. In *SAGA-Analyses and Modelling Applications*; Goltze: Göttingen, Germany, 2006.
79. Gallant, J.C.; Dowling, T.I. A Multiresolution Index of Valley Bottom Flatness for Mapping Depositional Areas. *Water Resour. Res.* **2003**, *39*, 1347. [CrossRef]

80. Böhner, J.; Koethe, R.; Conrad, O.; Gross, J.; Ringeler, A.; Selige, T. Soil Regionalisation by Means of Terrain Analysis and Process Parameterisation. *Soil Classif.* **2001**, *7*, 213.
81. Olaya, V.; Conrad, O. Geomorphometry in SAGA. *Dev. Soil Sci.* **2009**, *33*, 293–308.
82. Böhner, J.; Antonić, O. Land-Surface Parameters Specific to Topo-Climatology. *Dev. Soil Sci.* **2009**, *33*, 195–226.
83. Dietrich, H.; Böhner, J. Cold Air Production and Flow in a Low Mountain Range Landscape in Hessia (Germany). *Hambg. Beiträge Zur Phys. Geogr. Und Landschaftsökologie* **2008**, *19*, 37–48.
84. Beven, K.J.; Kirkby, M.J. A Physically Based, Variable Contributing Area Model of Basin Hydrology/Un Modèle à Base Physique de Zone d'appel Variable de l'hydrologie Du Bassin Versant. *Hydrol. Sci. J.* **1979**, *24*, 43–69. [CrossRef]
85. Naimi, B. USDM R Package: Uncertainty Analysis for Species Distribution Models (Version 2.1.7). 2023. Available online: https://cran.r-project.org/web/packages/usdm/index.html (accessed on 1 December 2023).
86. *R Core Team R: A Language and Environment for Statistical Computing*; Foundation for Statistical Computing: Vienna, Austria, 2023.
87. Cobos, M.E.; Peterson, A.T.; Osorio-Olvera, L.; Jiménez-García, D. An Exhaustive Analysis of Heuristic Methods for Variable Selection in Ecological Niche Modeling and Species Distribution Modeling. *Ecol. Inform.* **2019**, *53*, 100983. [CrossRef]
88. Thuiller, W.; Georges, G.; Engler, D.; Breiner, F. Biomod2: Ensemble Platform for Species Distribution Modelling (Version 4.2.0). 2023. Available online: https://cran.r-project.org/web/packages/biomod2/index.html (accessed on 1 December 2023).
89. Schwager, P.; Berg, C. Global Warming Threatens Conservation Status of Alpine EU Habitat Types in the Euro-pean Eastern Alps. *Reg. Environ. Change* **2019**, *19*, 2411–2421. [CrossRef]
90. Robinson, T.P.; Novelly, P.; Watson, I.; Corner, R.; Thomas, P.; Schut, T.; Jansen, S.; Shepherd, D. *Towards an Approach for Remote Sensing-Based Rangeland Condition Assessment in North Western Australia*; Surveying & Spatial Sciences Institute: Deakin, Australia, 2009; Volume 200, pp. 899–913.
91. Fielding, A.H.; Bell, J.F. A Review of Methods for the Assessment of Prediction Errors in Conservation Pres-ence/Absence Models. *Environ. Conserv.* **1997**, *24*, 38–49. [CrossRef]
92. Swets, J.A. Measuring the Accuracy of Diagnostic Systems. *Science* **1988**, *240*, 1285–1293. [CrossRef] [PubMed]
93. Hawkins, D.M. The Problem of Overfitting. *J. Chem. Inf. Comput. Sci.* **2004**, *44*, 1–12. [CrossRef]
94. DeLong, E.R.; DeLong, D.M.; Clarke-Pearson, D.L. Comparing the Areas under Two or More Correlated Receiver Operating Characteristic Curves: A Nonparametric Approach. *Biometrics* **1988**, *44*, 837–845. [CrossRef]
95. Robin, X.; Turck, N.; Hainard, A.; Tiberti, N.; Lisacek, F.; Sanchez, F.; Müller, M. pROC: An Open-Source Package for R and S+ to Analyse and Compare ROC Curves. *BMC Bioinform.* **2011**, *12*, 77. [CrossRef]
96. Merow, C.; Smith, M.J.; Silander Jr, J.A. A Practical Guide to MaxEnt for Modeling Species' Distributions: What It Does, and Why Inputs and Settings Matter. *Ecography* **2013**, *36*, 1058–1069. [CrossRef]
97. Elith, J.; Ferrier, S.; Huettmann, F.; Leathwick, J. The Evaluation Strip: A New and Robust Method for Plotting Predicted Responses from Species Distribution Models. *Ecol. Model.* **2005**, *186*, 280–289. [CrossRef]
98. Henckens, M.L.; van Ierland, E.C.; Driessen, P.P.; Worrell, E. Mineral Resources: Geological Scarcity, Market Price Trends, and Future Generations. *Resour. Policy* **2016**, *49*, 102–111. [CrossRef]
99. Hingston, F.; Dimmock, G.; Turton, A. Nutrient Distribution in a Jarrah (Eucalyptus Marginata Donn Ex Sm.) Ecosystem in South-West Western Australia. *For. Ecol. Manag.* **1980**, *3*, 183–207.
100. Roelofs, R.; Rengel, Z.; Cawthray, G.; Dixon, K.; Lambers, H. Exudation of Carboxylates in Australian Proteaceae: Chemical Composition. *Plant Cell Environ.* **2001**, *24*, 891–904. [CrossRef]
101. Bell, D.; Heddle, E. Floristic, Morphologic and Vegetational Diversity. In *The Jarrah Forest: A Complex Mediterranean Ecosystem*; Springer: Berlin/Heidelberg, Germany, 1989; pp. 53–66.
102. Koch, J.M. Restoring a Jarrah Forest Understorey Vegetation after Bauxite Mining in Western Australia. *Restor. Ecol.* **2007**, *15*, S26–S39. [CrossRef]
103. Jansen, S.; Broadley, M.R.; Robbrecht, E.; Smets, E. Aluminum Hyperaccumulation in Angiosperms: A Review of Its Phylogenetic Significance. *Bot. Rev.* **2002**, *68*, 235–269. [CrossRef]
104. O'connell, A.; Grove, T.; Dimmock, G. Nutrients in the Litter on Jarrah Forest Soils. *Aust. J. Ecol.* **1978**, *3*, 253–260. [CrossRef]
105. Lambers, H.; Juniper, D.; Cawthray, G.R.; Veneklaas, E.J.; Martínez-Ferri, E. The Pattern of Carboxylate Exudation in Banksia Grandis (Proteaceae) Is Affected by the Form of Phosphate Added to the Soil. *Plant Soil* **2002**, *238*, 111–122. [CrossRef]
106. Webb, L. Aluminium Accumulation in the Australian–New Guinea Flora. *Aust. J. Bot.* **1954**, *2*, 176–196. [CrossRef]
107. Hayward, M.W.; De Tores, P.J.; Fox, B.J. Post-Fire Vegetation Succession in Taxandria Linearifolia Swamps in the Northern Jarrah Forest of Western Australia. *Conserv. Sci. West. Aust.* **2008**, *7*, 35–42.
108. Corrick, M.G.; Fuhrer, B.A. *Wildflowers of Southern-Western Australia*; Five Mile Press: Elwood, Australia, 1996; in association with Monash University; ISBN 1-875971-49-1.
109. Crombie, D.; Tippett, J.; Hill, T. Dawn Water Potential and Root Depth of Trees and Understorey Species in Southwestern Australia. *Aust. J. Bot.* **1988**, *36*, 621–631. [CrossRef]
110. Crombie, D.S. Root Depth, Leaf Area and Daytime Water Relations of Jarrah (Eucalyptus Marginata) Forest Over-storey and Understorey during Summer Drought. *Aust. J. Bot.* **1992**, *40*, 113–122. [CrossRef]
111. Kopecký, M.; Macek, M.; Wild, J. Topographic Wetness Index Calculation Guidelines Based on Measured Soil Moisture and Plant Species Composition. *Sci. Total Environ.* **2021**, *757*, 143785. [CrossRef]

112. Freyssinet, P.; Butt, C.; Morris, R.; Piantone, P. *Ore-Forming Processes Related to Lateritic Weathering*; Society of Economic Geologists, Inc.: Littleton, CO, USA, 2005.
113. Qiu, Y.; Fu, B.; Wang, J.; Chen, L. Spatial Variability of Soil Moisture Content and Its Relation to Environmental Indices in a Semi-Arid Gully Catchment of the Loess Plateau, China. *J. Arid Environ.* **2001**, *49*, 723–750. [CrossRef]
114. De Reu, J.; Bourgeois, J.; Bats, M.; Zwertvaegher, A.; Gelorini, V.; De Smedt, P.; Chu, W.; Antrop, M.; De Maeyer, P.; Finke, P. Application of the Topographic Position Index to Heterogeneous Landscapes. *Geomorphology* **2013**, *186*, 39–49. [CrossRef]
115. Grubb, P.L.C. High-Level and Low-Level Bauxitization: A Criterion for Classification. *Miner. Sci. Eng.* **1973**, *5*, 219–223.
116. Baker, G.F.U. Darling Range Bauxite Deposits. Economic Geology of Australia and Papua New Guinea. *Aust. Inst. Min. Metall.* **1975**, *5*, 980–986.
117. Wibowo, S.; Rosana, M.F.; Haryanto, A.D. Local Topographic Model Using Position Index for Analyzing the Characteristics of Unserpentinized Lateritic Zones in Sorowako Nickeliferous Laterite Deposit, Indonesia. *Int. J. Adv. Sci. Eng. Inf. Technol.* **2018**, *8*, 1138. [CrossRef]
118. Guisan, A.; Thuiller, W.; Zimmermann, N.E. *Habitat Suitability and Distribution Models: With Applications in R*; Cambridge University Press: Cambridge, UK, 2017; ISBN 0-521-76513-7.
119. Beaudette, D.E.; Dahlgren, R.A.; O'Geen, A.T. Terrain-shape Indices for Modeling Soil Moisture Dynamics. *Soil Sci. Soc. Am. J.* **2013**, *77*, 1696–1710. [CrossRef]
120. Li, X.; McCarty, G.W.; Karlen, D.L.; Cambardella, C.A. Topographic Metric Predictions of Soil Redistribution and Organic Carbon in Iowa Cropland Fields. *Catena* **2018**, *160*, 222–232. [CrossRef]
121. Khan, S.M.; Page, S.; Ahmad, H.; Harper, D. Identifying Plant Species and Communities across Environmental Gradients in the Western Himalayas: Method Development and Conservation Use. *Ecol. Inform.* **2013**, *14*, 99–103. [CrossRef]
122. Solon, J.; Degórski, M.; Roo-Zielińska, E. Vegetation Response to a Topographical-Soil Gradient. *Catena* **2007**, *71*, 309–320. [CrossRef]
123. Ahmad, Z.; Khan, S.M.; Page, S.; Alamri, S.; Hashem, M. Plants Predict the Mineral Mines–A Methodological Approach to Use Indicator Plant Species for the Discovery of Mining Sites. *J. Adv. Res.* **2022**, *39*, 119–133. [CrossRef]
124. Hofton, M.; Dubayah, R.; Blair, J.B.; Rabine, D. Validation of SRTM Elevations over Vegetated and Non-Vegetated Terrain Using Medium Footprint Lidar. *Photogramm. Eng. Remote Sens.* **2006**, *72*, 279–285. [CrossRef]
125. Wang, Z.Z.; Hu, Y.; Guo, X.; He, X.; Kek, H.Y.; Ku, T.; Goh, S.H.; Leung, C.F. Predicting Geological Interfaces Using Stacking Ensemble Learning with Multi-Scale Features. *Can. Geotech. J.* **2023**, *60*, 1036–1054. [CrossRef]
126. Zhang, L.; Huettmann, F.; Liu, S.; Sun, P.; Yu, Z.; Zhang, X.; Mi, C. Classification and Regression with Random Forests as a Standard Method for Presence-Only Data SDMs: A Future Conservation Example Using China Tree Species. *Ecol. Inform.* **2019**, *52*, 46–56. [CrossRef]
127. Hao, T.; Elith, J.; Guillera-Arroita, G.; Lahoz-Monfort, J.J. A Review of Evidence about Use and Performance of Species Distribution Modelling Ensembles like BIOMOD. *Divers. Distrib.* **2019**, *25*, 839–852. [CrossRef]
128. Kaky, E.; Nolan, V.; Alatawi, A.; Gilbert, F. A Comparison between Ensemble and MaxEnt Species Distribution Modelling Approaches for Conservation: A Case Study with Egyptian Medicinal Plants. *Ecol. Inform.* **2020**, *60*, 101150. [CrossRef]
129. Hao, T.; Elith, J.; Lahoz-Monfort, J.J.; Guillera-Arroita, G. Testing Whether Ensemble Modelling Is Advantageous for Maximising Predictive Performance of Species Distribution Models. *Ecography* **2020**, *43*, 549–558. [CrossRef]
130. Valavi, R.; Guillera-Arroita, G.; Lahoz-Monfort, J.J.; Elith, J. Predictive Performance of Presence-only Species Dis-tribution Models: A Benchmark Study with Reproducible Code. *Ecol. Monogr.* **2022**, *92*, e01486. [CrossRef]
131. Hronsky, J.M.; Kreuzer, O.P. Applying Spatial Prospectivity Mapping to Exploration Targeting: Fundamental Practical Issues and Suggested Solutions for the Future. *Ore Geol. Rev.* **2019**, *107*, 647–653. [CrossRef]
132. Zuo, R. Geodata Science-Based Mineral Prospectivity Mapping: A Review. *Nat. Resour. Res.* **2020**, *29*, 3415–3424. [CrossRef]
133. Meyer, F. Availability of Bauxite Reserves. *Nat. Resour. Res.* **2004**, *13*, 161–172. [CrossRef]
134. Momo, M.N.; Yemefack, M.; Tematio, P.; Beauvais, A.; Ambrosi, J.-P. Distribution of Duricrusted Bauxites and Laterites on the Bamiléké Plateau (West Cameroon): Constraints from GIS Mapping and Geochemistry. *Catena* **2016**, *140*, 15–23. [CrossRef]
135. Ouyang, Y.; Liu, H.; Wang, X.; Liu, S.; Zhang, J.; Gao, H. Spatial Distribution Prediction of Laterite Bauxite in Bo-laven Plateau Using GIS. *J. Earth Sci.* **2019**, *30*, 1010–1019. [CrossRef]
136. *GSWA 1:50,000 State Interpreted Bedrock Geology of Western Australia*; Geological Survey of Western Australia: Perth, Australia, 2021.
137. Kalinowski, A.; Oliver, S. ASTER Mineral Index Processing Manual. *Remote Sens. Appl. Geosci. Aust.* **2004**, *37*, 36–37.
138. Anifadi, A.; Sykioti, O.; Koutroumbas, K.; Vassilakis, E. A Novel Spectral Index for Identifying Ferronickel (Fe–Ni) Laterites from Sentinel 2 Satellite Data. *Nat. Resour. Res.* **2022**, *31*, 1203–1224. [CrossRef]
139. Sabins, F.F. Remote Sensing for Mineral Exploration. *Ore Geol. Rev.* **1999**, *14*, 157–183. [CrossRef]
140. Chung, C.-J.; Keating, P.B. Mineral Potential Evaluation Based on Airborne Geophysical Data. *Explor. Geophys.* **2002**, *33*, 28–34. [CrossRef]
141. Milligan, P.; Minty, B.; Richardson, M.; Franklin, R. The Australia-Wide Airborne Geophysical Survey-Accurate Continental Magnetic Coverage. *ASEG Ext. Abstr.* **2009**, *2009*, 1–9. [CrossRef]

142. Hernandez, P.A.; Graham, C.H.; Master, L.L.; Albert, D.L. The Effect of Sample Size and Species Characteristics on Performance of Different Species Distribution Modeling Methods. *Ecography* **2006**, *29*, 773–785. [CrossRef]
143. McCune, J. Species Distribution Models Predict Rare Species Occurrences despite Significant Effects of Landscape Context. *J. Appl. Ecol.* **2016**, *53*, 1871–1879. [CrossRef]